

## Chapter 4: The Aluminium Magnesium Boron Ternary Phase Diagram

### 4.1: Introduction

In this chapter the aluminium-magnesium-boron ternary phase diagram will be addressed. In general it is important to have a detailed understanding of the respective phase diagram from which a specific material needs to be processed. More specifically, the processing of  $\text{AlMgB}_{14}$  requires a fundamental understanding of the Al-Mg-B phase diagram. Very little is known about the Al-Mg-B phase diagram and so it, together with the binary systems Al-B and Mg-B, will be introduced in this chapter. For a more detailed description of the theory behind phase diagrams the reader is referred to Bergeron and Risbud<sup>43</sup>.

#### 4.1.1: The Aluminium-Boron Binary Phase Diagram

The Al-B binary system is given in figure 4.1.1.

There is no measurable solid solution that forms between aluminium and boron<sup>44</sup>. Boron is allotropic and can form an  $\alpha$  and a  $\beta$  form. The  $\alpha$  allotrope is formed by the deposition of vapourised boron at 1000°C and once deposited forms the  $\beta$  allotrope when heated to 1300°C<sup>45</sup>.  $\text{AlB}_{12}$  has two polymorphs with an  $\alpha \rightarrow \beta$  transformation occurring at 1550°C. The peritectic reaction of  $\text{L} + \beta\text{-AlB}_{12} \leftrightarrow \text{AlB}_{10}$  has been used to explain the thermal arrest at 1850°C<sup>46</sup>.  $\text{AlB}_{10}$  was identified in compositions quenched from temperatures of 1660°C and 1850°C<sup>47</sup>. Nernov found that the  $\beta\text{-AlB}_{12}$  and  $\text{AlB}_{10}$  are stabilised by impurities and that these phases do not exist unless so stabilised<sup>48</sup>. Figure 4.1.1 shows the Al-B binary system.

Of specific interest to this study is the compound  $\text{AlB}_2$  since  $\text{AlB}_2$  and  $\text{MgB}_2$ , form a solid solution.  $\text{AlB}_2$  is stable up to temperatures of 980°C. Above this temperature  $\text{AlB}_2$  decomposes into Al liquid and  $\text{AlB}_{12}$ .

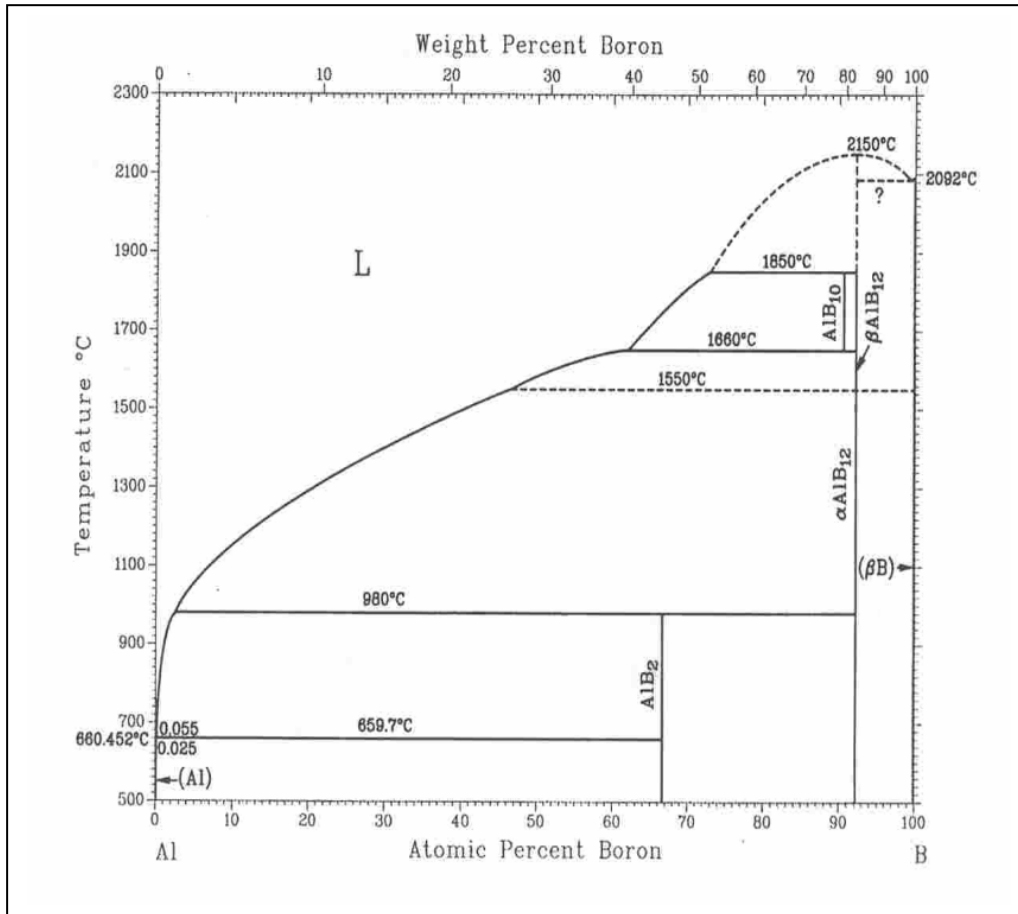


**Figure 4.1.1:** The aluminium-boron binary phase diagram reproduced from the review of the Al-B system given by O. N. Carlson<sup>49</sup>

The structural data for the phases in the Al-B binary phase diagram are given in table 4.1.1.

**TABLE 4.1.1:** Structural data for phases in the Al-B system

Phase/Temperature Range (°C)	Crystal System	Lattice Parameters (Å)	Reference JCPDS
Al/ < 660	Cubic	a = 4.039	03-0932
$\alpha$ -B/<1300	Hexagonal (R3m)	a = 5.057, $\alpha$ =58.060	85-0702
$\beta$ -B/ < 2092	Rhombohedral	a = 10.925, c = 23.814,	31-0207
AlB <sub>2</sub> / <980	Hexagonal	a = 3.0054, c = 3.25276	39-1483
AlB <sub>10</sub> / 1850	Rhombohedral	a = 7.835, c = 15.91,	22-0002
$\alpha$ -AlB <sub>12</sub> / 1550	Tetragonal	a = 10.16, c = 14.28,	12-0640
$\beta$ -AlB <sub>12</sub> / 2150	Orthorhombic	a = 10.925, b = 12.63 c = 23.814,	12-0639

#### ***4.1.2: The Magnesium-Boron Binary Phase Diagram***

The Mg-B system is fraught with inconsistent data<sup>50</sup>. Solid solubility of boron and magnesium in each other is negligible. The most magnesium rich phase is MgB<sub>2</sub> and the most boron rich phase has been proposed to be MgB<sub>12</sub>. MgB<sub>12</sub> however has never been isolated and fully characterised<sup>51</sup>. Several additional phases exist between these two boundary phases. They are MgB<sub>4</sub> and MgB<sub>7</sub>. The stability of these phases has only been calculated and are shown in figure 4.1.2, reproduced from the work of Nayeb-Hashemi<sup>50</sup>.

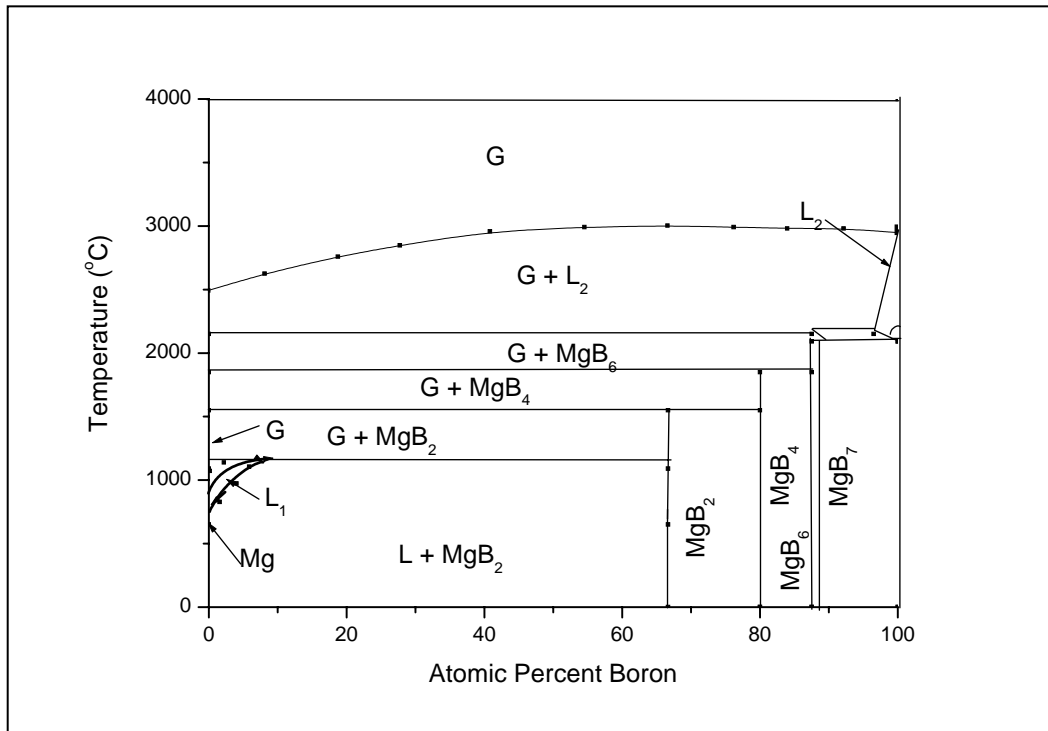


**Figure 4.1.2:** The magnesium-boron binary phase diagram<sup>50</sup>

**TABLE 4.1.2:** Structural data for the phases in the Mg-B system

Phase/Temperature Range (°C)	Crystal System	Lattice Parameters (Å)	Reference JCPDS
Mg/ < 649°C	Hexagonal	a = 3.20936	35-0821
β-B/ < 2092°C	Rhombohedral	a = 10.925, c = 23.814	31-0207
MgB <sub>2</sub> / < 1600°C	Hexagonal	a = 3.0864, c = 3.5215	38-1369
MgB <sub>4</sub> / 1850°C	Orthorhombic	a = 5.464, b = 7.472, c = 15.91	15-0299
MgB <sub>6</sub> / 2120°C	Tetragonal	a = 10.16, c = 14.28	12-0640
MgB <sub>7</sub>	Orthorhombic	a = 5.970, b = 8.125, c = 10.480	*10
MgB <sub>20</sub>	Trigonal	a = 10.983, c = 24.156	*9

\* referenced from the literature

Table 4.1.2 summarises the structural data for the phases identified in figure 4.1.2.

The structural formula of  $\text{MgB}_7$  is  $\text{Mg}_2\text{B}_{14}$ . It has been determined from X-ray powder patterns by a refinement technique and its structure is based on the structure  $\text{AlMgB}_{14}$ <sup>52</sup>. The refinement was based on the *Imam* space group. The structure consists of boron icosahedral chains that extend along the c axis and are linked laterally via inter-icosahedral bonds involving B atoms that are themselves non-icosahedral.

$\text{MgB}_{20}$  was only recently discovered as a new phase in the Mg-B binary phase system<sup>53</sup>. Insufficient thermodynamic data is known about this phase and so it has not been included in the Mg-B binary phase diagram presented in figure 4.1.2. This phase was discovered by Brutti *et al* in an attempt to isolate  $\text{MgB}_{12}$ <sup>51</sup>. The synthesis procedure to prepare  $\text{MgB}_{20}$  involved heating Mg and B in the atomic ratio of 1:12 respectively to 1150°C. Two phases were isolated from this reaction  $\text{MgB}_7$  and a much richer boron Mg-B phase. Through refinement and ICP studies on the purified boron rich Mg-B phase the chemical formula of  $\text{MgB}_{20}$  was found to be the stoichiometry of this new phase.

#### ***4.1.3: The Al-Mg Binary System***

The Al-Mg binary phase system is well documented in the literature<sup>53</sup>. The maximum solid solubility of magnesium in aluminium is 18.9 at.% at a eutectic temperature of 450°C. The maximum solid solubility of aluminium in magnesium is 11.8 at.% at a eutectic temperature of 437°C. The compound  $\text{Al}_3\text{Mg}_2$  has a complex fcc structure at low temperatures. As the temperature is increased this compound undergoes a martensitic transformation but this has not been studied in detail<sup>56</sup>. The compound  $\text{Al}_{12}\text{Mg}_{17}$  can have a composition range of approximately 45 to 60.5 at.% Mg. However the ideal crystal structure has the stoichiometry  $\text{Al}_{12}\text{Mg}_{17}$ . The binary phase diagram is reproduced in figure 4.1.3 and the associated crystallographic information is presented in table 4.1.3.

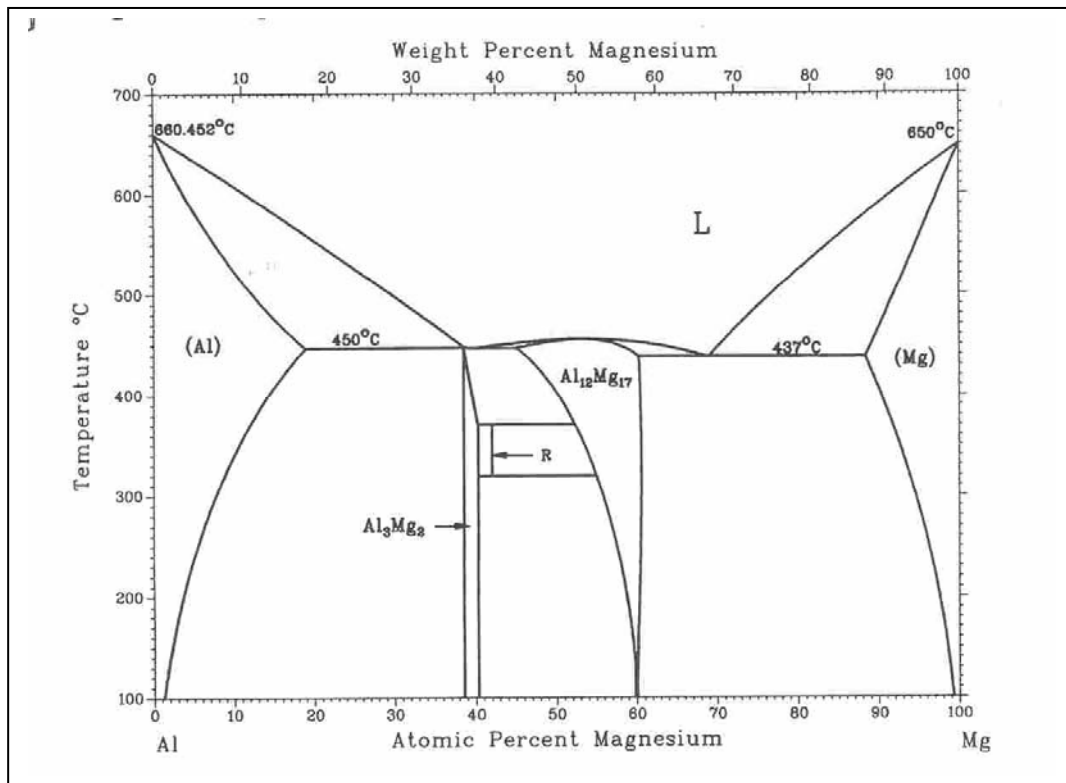


**Figure 4.1.3:** The Al-Mg binary phase diagram<sup>53</sup>

**TABLE 4.1.3:** Structural data for the phases in the Al-Mg binary phase diagram

Phase/Temperature Range (°C)	Crystal System	Lattice Parameters (Å)	Reference JCPDS
Al/ < 660	Cubic	a = 4.049	04-0787
Al <sub>3</sub> Mg <sub>2</sub> / < 450	Hexagonal	a = 5.7500, c = 9.5400	40-0903
R = Al <sub>2</sub> Mg <sub>3</sub> / < 370	Hexagonal	a = 7.650, c = 19.850	44-1154
Al <sub>12</sub> Mg <sub>17</sub> / < 450	Cubic	a = 10.560	01-1128
Mg/ 649	Hexagonal	a = 3.209, c = 5.211	35-0821

#### ***4.1.4: The Aluminium-Magnesium-Boron Ternary Phase Diagram***

Early studies on this system dealt mostly with boron as a grain refining additive to Al-Mg alloys<sup>54</sup>. No complete phase diagram has been determined for this ternary system. A great deal of interest in the ternary system has largely been devoted to the study of the hard compound  $\text{AlMgB}_{14}$ <sup>2,3,22,55,56</sup>.

Preparative routes to synthesise single crystals of  $\text{AlMgB}_{14}$  from aluminium rich fluxes with a starting composition of  $\text{MgAl}_{31}\text{B}_6$  was done by heating this composition under argon in an alumina crucible to 1500°C. The solution was kept at this temperature for 1 hour and then cooled at 10°Cmin<sup>-1</sup> to room temperature. The excess aluminium was leached out with hot HCl. Matkovich<sup>3</sup> *et. al.* prepared  $\text{AlMgB}_{14}$  from the starting composition of  $\text{MgAl}_2\text{B}_{14}$  by heating it at 900°C for 6 hours.

The most extensive study on the phase diagram was performed by Vekshina<sup>6</sup>. Samples were prepared from pure boron (99.2%), magnesium (99.9%) and aluminium (99.9%). Twenty two ternary alloys were synthesised and characterised by XRD. Despite kinetic difficulties, a solid solution between  $\text{AlB}_2$  and  $\text{MgB}_2$  was found to form at temperatures of between 725°C and 790°C<sup>5</sup>. A tentative isothermal section is drawn in figure 4.1.4 for the Al-Mg-B system at 900°C based on the review on this ternary system given by Ran<sup>57</sup>.

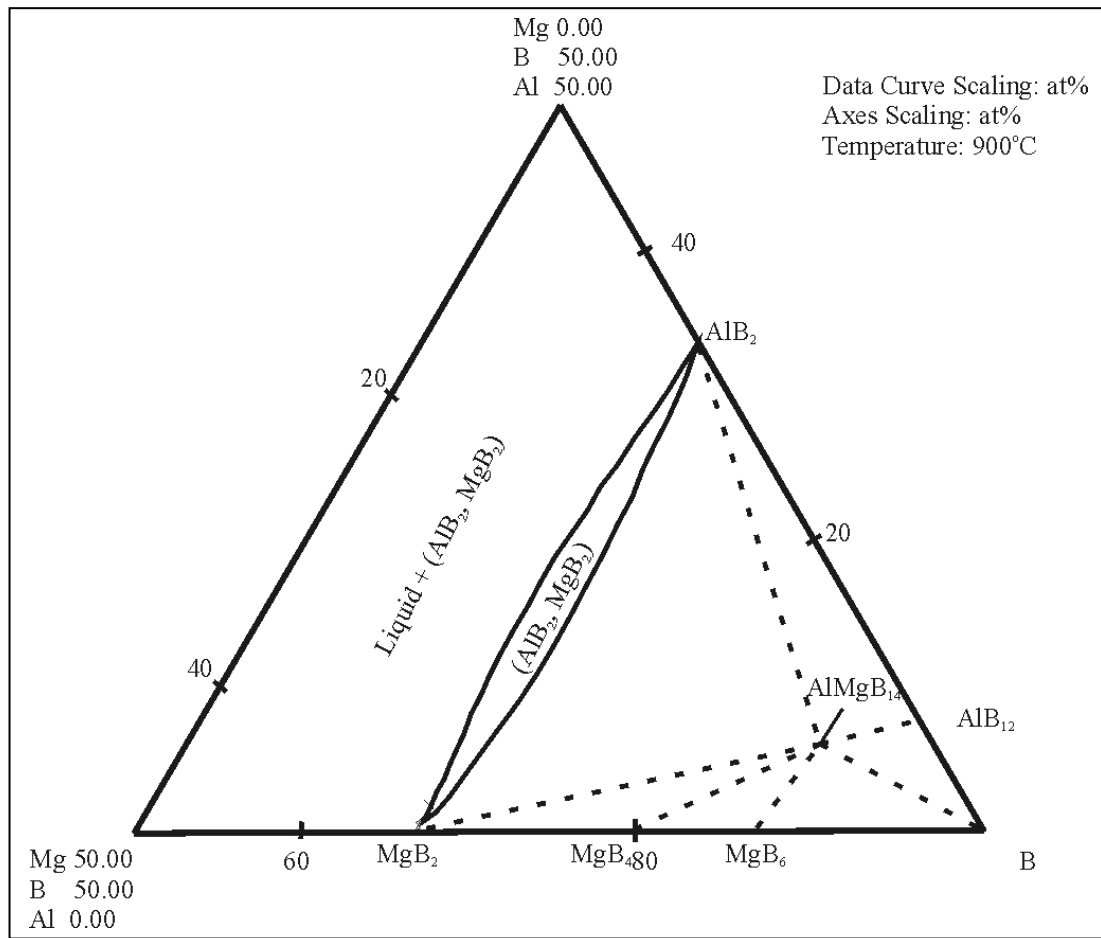


**Figure 4.1.4:** An isothermal section of the Al-Mg-B ternary phase diagram at 900°C<sup>57</sup>

Table 4.1.4 summarises the crystal data for the AlMgB<sub>14</sub> and the solid solution phase (Al, Mg)B<sub>2</sub> phase which are the only outstanding phases from the summary tables presented for the Al-B and Mg-B systems.

**TABLE 4.1.4:** Structural data of AlMgB<sub>14</sub>

Phase/Temperature Range (°C)	Crystal System	Lattice Parameters (Å)	Reference JCPDS
*AlMgB <sub>14</sub>	Orthorhombic	a = 5.8480, b = 8.1120, c = 10.3120	39-0459

\* substoichiometric (Al<sub>0.75</sub>Mg<sub>0.78</sub>B<sub>14</sub>)<sup>22</sup>

#### ***4.1.5: The Solid Solution***

As discussed earlier the existence of a solid solution between  $\text{AlB}_2$  and  $\text{MgB}_2$  in the Al-Mg-B system is expected. A preliminary observation from the phase diagrams presented in figures 4.1.1 and 4.1.2 indicates that  $\text{AlB}_2$  is stable up to temperatures of  $980^\circ\text{C}$  and  $\text{MgB}_2$  up to  $1600^\circ\text{C}$ . The decomposition of the  $\text{AlB}_2$  phase at  $980^\circ\text{C}$  suggests that the solid solution phase in the ternary system at temperatures above  $980^\circ\text{C}$  will not be continuous and that the solid solution boundary should move towards more magnesium rich solid solutions.

It is possible to calculate the position of the solid solution boundary using Rietveld refinement techniques by working out the cell parameters of the solid solution phase for a given composition point preferably somewhere near to the solid solution boundary<sup>58</sup>. Once the cell parameters of the solid solution phase have been determined the composition of the solid solution phase can be calculated by using Vegard's law. Vegard's law states that the change in the lattice parameter for a continuous solid solution is directly proportional to the atomic percent of the solute present. As shown in figure 4.1.4 such a continuous solid solution exists between  $\text{AlB}_2$  and  $\text{MgB}_2$  for temperatures below  $900^\circ\text{C}$ . Therefore, by judicious choice of compositions around the solid solution boundary the composition of the solid solution boundary can be calculated.

The calculation of the cell parameters is described in section 4.2.2. In particular a shift in the value of  $2\theta$  or d-space for a solid solution phase directly translates into a change in the composition of the solid solution phase. It is therefore possible to decide whether the composition of a solid solution is changing by determining the shift in the value of  $2\theta$  or d-space for a given diffraction plane. The direction of the shift with respect to the pure phases of that solid solution indicates the direction in which the composition of the solid solution moves.

## **4.2: Experimental**

Powders of the various compositions in order to produce  $\text{AlMgB}_{14}$  were prepared as laid out in the experimental chapter 3. For purposes of convenience the method employed for calculating the lattice parameters from the XRD data will be presented in this experimental section. All the XRD data were determined post reaction and therefore reported temperatures refer to the synthesis temperature and not the temperature at which the XRD was run.

Phase analysis was done by using XRD (Cu  $K\alpha$  radiation) and the observed peaks were matched using the JCPDS database. In addition to this Rietveld analysis was done in order to determine the cell parameters for the solid solution and to quantify the phases present. A description of the XRD equipment used is given in the experimental chapter, Chapter 3, section 3.4.4.

### **4.2.1: Qualitative XRD analysis**

Qualitative XRD analysis was done in order to identify the phases present in the material. This was done by running a powdered sample in the XRD at step sizes of  $0.04^\circ 2\theta$  and 5 second count times. The resulting diffractogram for that sample was then analysed using X'Pert high score software developed by Phillips.

### **4.2.2: Quantitative XRD analysis**

High purity silicon was used as an internal standard in the XRD analysis. 5% by mass of silicon was added to each composition by physically mixing (with pestle and mortar) the silicon into the sample powder until the resultant mixture was homogeneous. For example, figure 4.2.1 shows the diffractogram for a composition of Al, Mg and B prepared at  $900^\circ\text{C}$  after the addition of the internal standard.

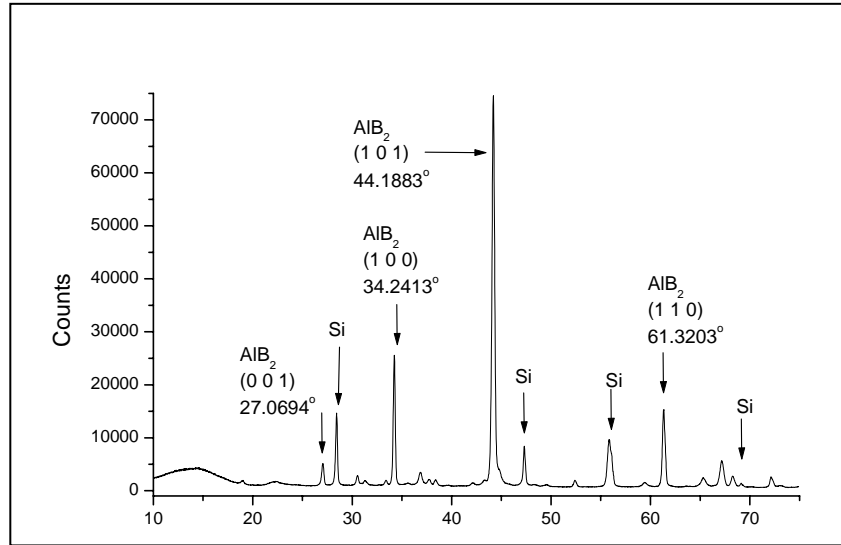


**Figure 4.2.1:** XRD pattern for composition 1 at 900°C with 5 wt% silicon as an internal standard

#### 4.2.2: The XRD Scan Criteria

In order to maximise the number of diffraction planes to reduce the error in the estimation of the cell constants from the XRD data, peaks over a wide range of angles were recorded. Table 4.2.1 lists the peaks expected from AlB<sub>2</sub>, MgB<sub>2</sub> and their suitability for analyses.

**TABLE 4.2.1:** 2 Theta peaks for AlB<sub>2</sub>, MgB<sub>2</sub>

			AlB <sub>2</sub> Card: 39-1483	MgB <sub>2</sub> Card: 38-1369	Intensity		Suitability
h	k	l	2θ	2θ	AlB <sub>2</sub>	MgB <sub>2</sub>	*
0	0	1	27.418	25.266	12	4	
1	0	0	34.414	33.483	34	26	
1	0	1	44.542	42.412	100	100	
1	1	0	61.695	59.886	24	21	
1	0	2	67.907	63.173	8	5	
1	1	1	68.77	66.045	4	5	
2	0	0	72.56	70.403	4	4	**
2	0	1	79.219	76.126	12	11	*

1	1	2	88.514	83.191	10	11	*
1	0	3	100.639	91.591	5	6	*
2	1	1	109.78	104.963	8	9	*
2	0	3	135.248	121.735	<1	2	*

\*peaks partially overlap with the internal standard

\*\* peak partially overlaps with MgAl<sub>2</sub>O<sub>4</sub>

XRD scans were run at 0.01°/step at a count time of 10s per step. From the above tables diffractograms were taken over the range 24-35° 2θ, 41.5-57.5 ° 2θ, 59-80 ° 2θ and 82-116 ° 2θ. Peak assignments were made for the solid solution and silicon peaks. From the assignments for the silicon peaks the diffractograms were shifted by finding a linear least squares fit from the plot of the measured 2θ values (y-axis) and the theoretical 2θ values (x-axis) for silicon. Figure 4.2.2 shows the linear fit the data for one sample, called composition 1 at 900°C. Composition 1 will be defined in section 4.3.1.

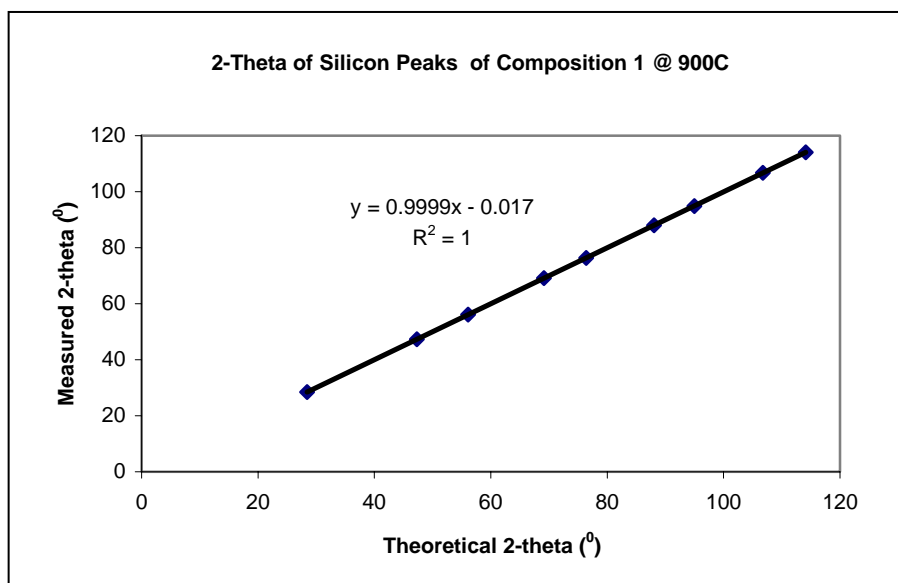


**Figure 4.2.2:** Linear equation for the shifting of the diffractogram for composition 1

From the equation generated the position of the shifted peaks were calculated. From the Bragg law, equation 4.1, the d-spacing for each shifted peak was calculated.

$$n\lambda = 2d \sin \theta \quad 4.1$$

From the d-spacing,  $1/d^2$  was calculated. The value of  $1/d^2$  was then used in equation 4.2 to estimate the values of the cell constants ‘a’ and ‘c’ for the hexagonal lattice using linear regression analysis by treating  $1/d^2$  as dependant on the independent values of  $h^2 + k^2 + l^2$ .

$$\frac{1}{d^2} = \frac{4}{3a^2} (h^2 + k^2 + hk) + \frac{l^2}{c^2} \quad 4.2$$

Table 4.2.2 lists the values of  $1/d^2$  calculated and  $1/d^2$  determined from linear regression analysis, hereafter referred to as  $1/d^2$  experimental, and the corresponding difference between the two values for composition 1 at 900°C.

**TABLE 4.2.2:** Values of  $1/d^2$  calculated and  $1/d^2$  experimental

			Comp.1	Sample 900°C				
Card 39- 1483		Exp. Intensity		Calc.			1000* $1/d^2$ experimental	Diff.
Intensity	I/I <sub>0</sub>	counts	AlB <sub>2</sub>	1000*1/ $d^2$	$4/3*(h^2+k^2+hk)$	$l^2$		
12	5	155	27.0760	92.35	0.00	1.00	92.36	0.01
34	34	1124	34.2512	146.14	1.33	0.00	145.85	0.28
100	100	3319	44.1848	238.39	1.33	1.00	238.21	0.18
24	22	737	61.2831	437.78	4.00	0.00	437.56	0.22
8	7	227	67.1409	515.31	1.33	4.00	515.28	0.03
4	3	99	68.1920	529.61	4.00	1.00	529.92	-0.30
4	3	103	72.0782	583.36	5.33	0.00	583.41	-0.05

The difference between all the experimentally determined values of  $1/d^2$  and the calculated values of  $1/d^2$  are all less than 0.3. The error in these measurements will be

addressed in more detail in the quantitative phase analysis section 4.3.5. This method will be referred to as method 1.

#### ***4.2.3: The Rietveld Method***

The phase composition of each of the compositions were measured by X-ray diffraction. The diffractometer that was used is a XRD 7 Seifert FPM. The step size used was 0.02 for the range 12-110° with a count time of 10 seconds per step. The quantification and determination of the lattice parameter was done using the software package AUTOQUAN supplied by Seifert FPM using the structural data given in the ICSD database. The R values from the refinement were in the range of 8-10%. For a more accurate determination of the lattice parameter Si was used as an internal standard. The standard deviation of the lattice parameter of the solid solution was less than  $5 \times 10^{-5}$  nm for both the a and c parameter. This method will be referred to as the Rietveld method.



The various compositions were specifically chosen to probe the solid solution boundary compositions. Thus compositions 1-3 were chosen to lie within the solid solution. Additionally, compositions 4-6 and compositions 8 and 9 lying either side of the solid solution, were chosen. Composition 10 was chosen in order to determine at what temperatures  $\text{AlMgB}_{14}$  can be made from the composition  $\text{AlMgB}_{14}$ . The ternary phase diagram as depicted in figure 4.3.1 is the boron rich corner of the triangle as both the other vertex points represent 50 at% each of the respective metals, Al and Mg. Table 4.3.1 lists the atomic percent of each of the constituents for each of the compositions depicted in figure 4.3.1.

**TABLE 4.3.1:** Atomic percent for the compositions

<b>Composition</b>	<b>Atomic Percent</b>		
	<b>Mg (%)</b>	<b>Al (%)</b>	<b>B (%)</b>
<b>1</b>	5.34	28.19	66.47
<b>2</b>	9.93	23.54	66.53
<b>3</b>	14.29	19.29	66.43
<b>4</b>	5.38	34.43	60.19
<b>5</b>	9.92	30.36	59.72
<b>6</b>	14.39	25.47	60.14
<b>7</b>	2.68	42.63	54.69
<b>8</b>	5.34	19.51	75.15
<b>9</b>	21.47	3.98	74.55
<b>10</b>	6.25	6.25	87.50

Samples of each composition, listed in table 4.3.1, were prepared at temperatures of 900°C, 1000°C, 1200°C and 1400°C. XRD was used for the identification of the crystalline phases in the materials.

### 4.3.2: Results of the Qualitative Analysis

The diffractogram for composition 1, at 900°C, together with the peak assignment is presented in figure 4.3.2 a. Composition 1 at 1000°C, 1200°C and 1400°C are represented in figures 4.3.2 b, c and d.

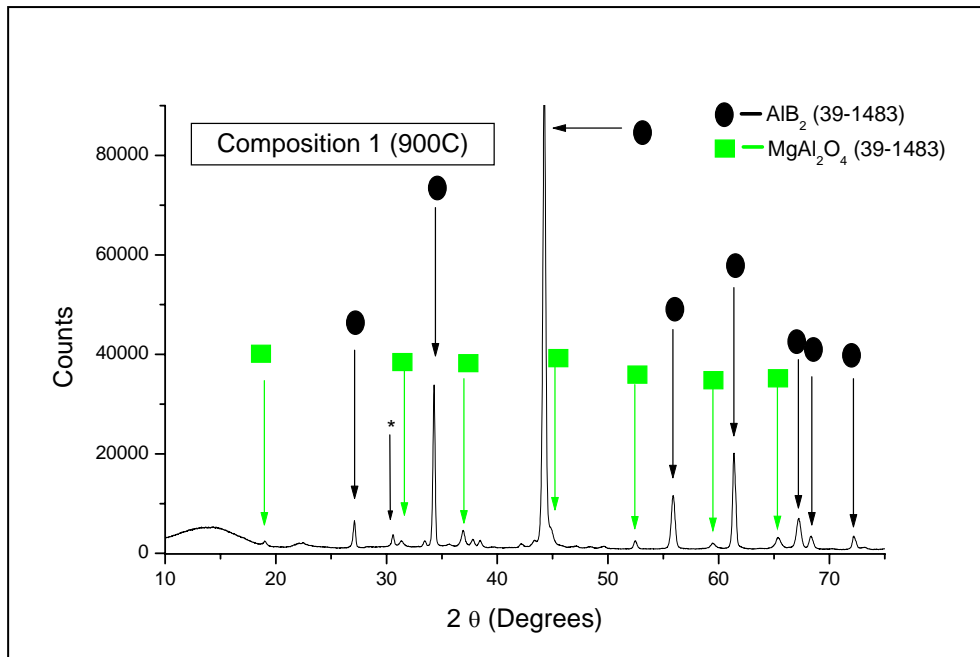


Figure 4.3.2 a: Diffractogram for composition 1 at 900°C

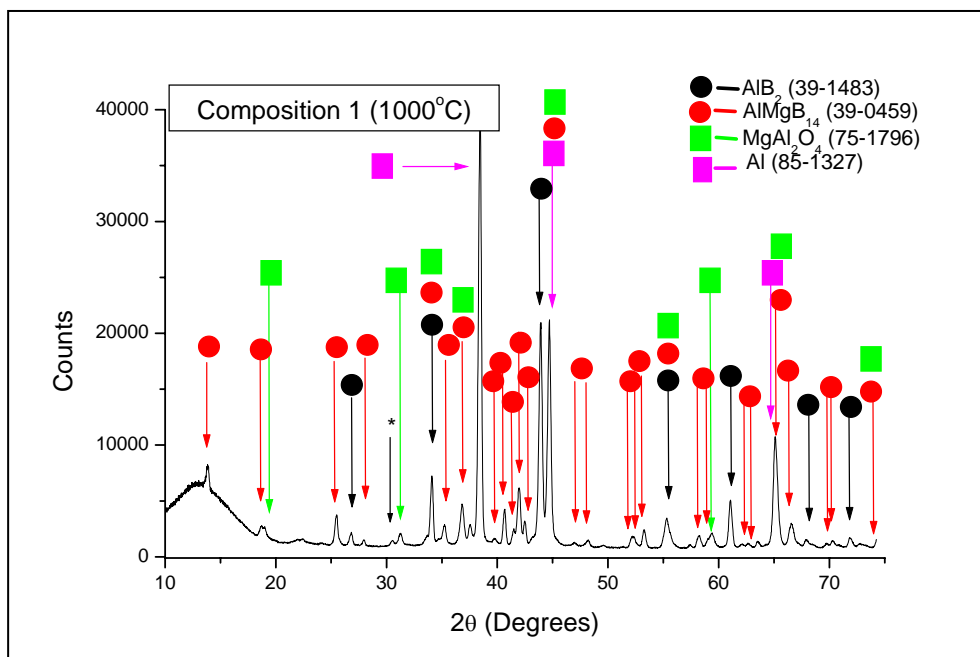


Figure 4.3.2 b: Diffractogram for composition 1 at 1000°C

The XRD peak indicated with a \* ( $30.51^\circ$ ) has not been identified. The relative intensity of this peak is 2.71. In figure 4.3.2 a this peak is noticeable and is adjacent to the spinel peak at  $31.27^\circ$ . Trace amounts of the unidentified phase are present because the peak heights are very small with respect to the major solid solution phase.

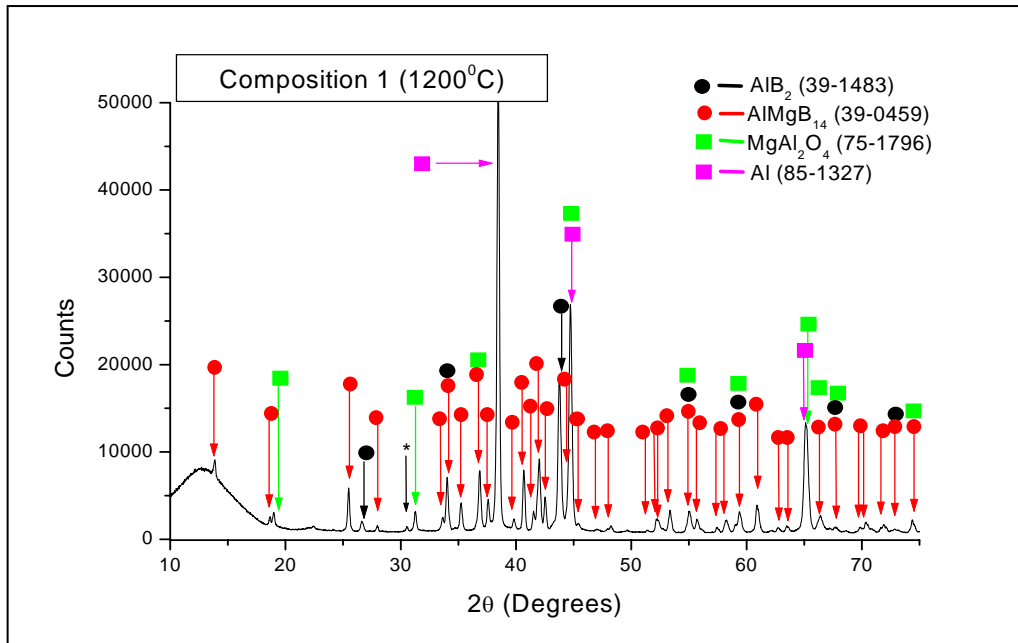


Figure 4.3.2 c: Diffractogram for composition 1 at 1200°C

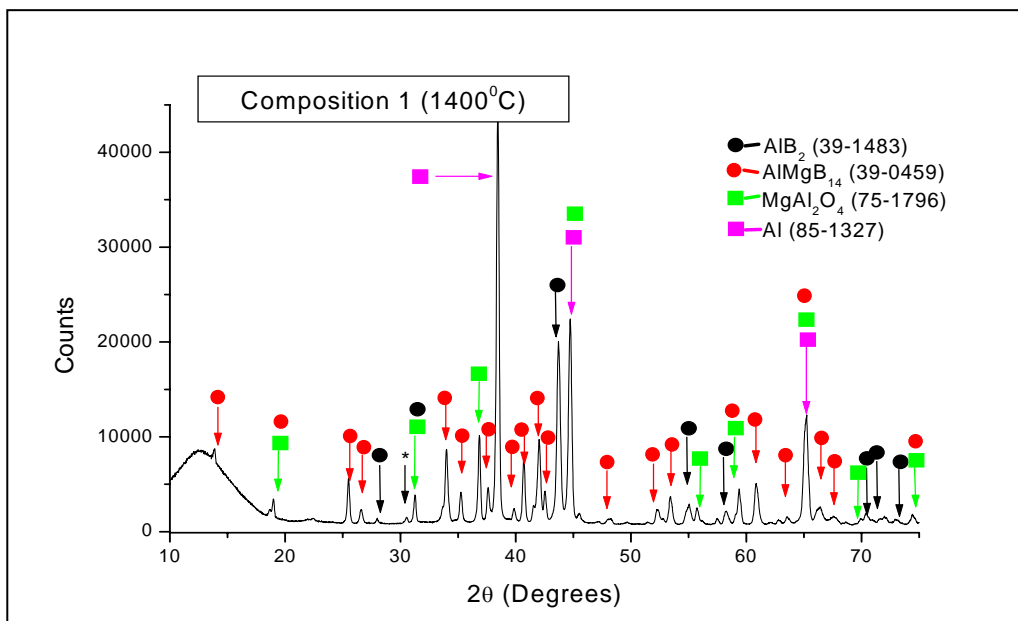
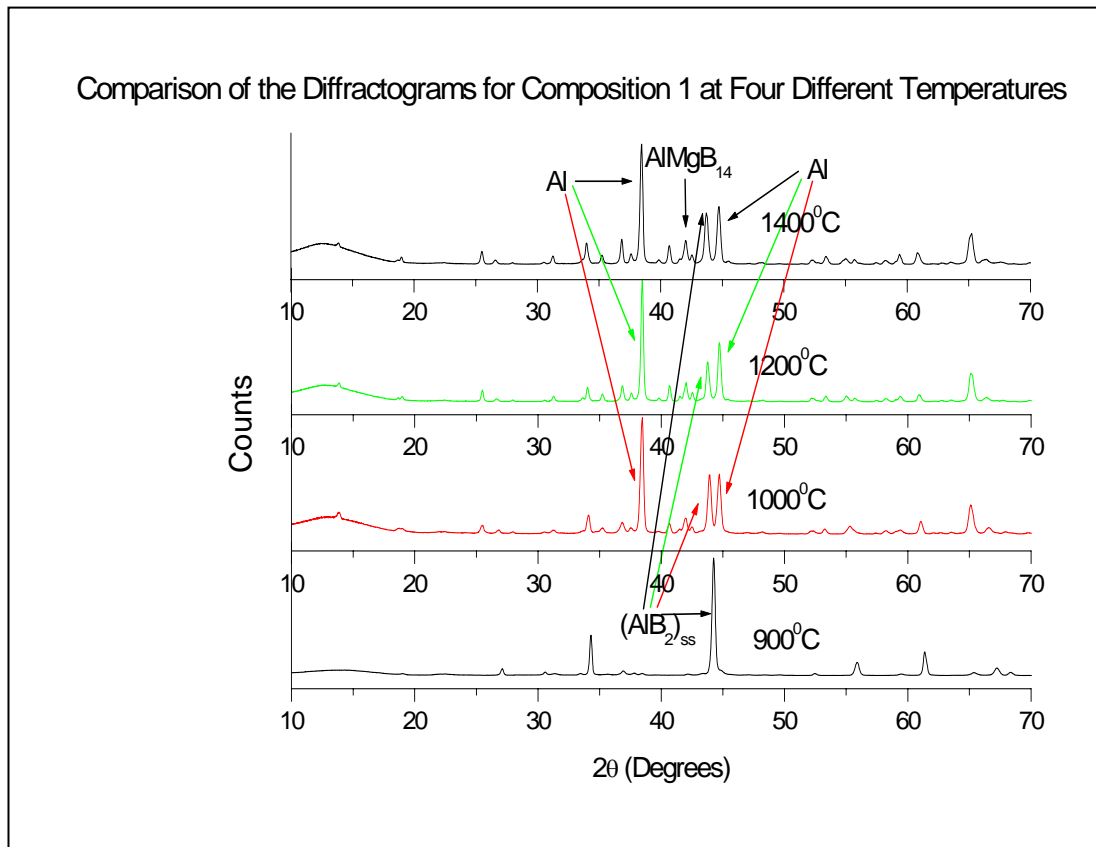


Figure 4.3.2 d: Diffractogram for composition 1 at 1400°C



**Figure 4.3.3:** Comparison of the diffractograms for composition 1

Figure 4.3.3 shows the four diffractograms collected for composition 1 at the four different temperatures and indicates the different phases quite clearly. The major peaks for the important phases are labelled in figure 4.3.3.

Aluminium and  $\text{AlMgB}_{14}$  are formed at temperatures greater than  $1000^{\circ}\text{C}$  for composition 1. Below  $1000^{\circ}\text{C}$  the solid solution phase together with the spinel phase are the only detectable phases. As the temperature is increased from  $900^{\circ}\text{C}$  to  $1400^{\circ}\text{C}$  the position of the XRD peaks for the solid solution phase shift to lower  $2\theta$  angles. The reason for the direction of the shift is that as the temperature is increased the solid solution decomposes, releasing Al and B. Thus, the lattice parameter associated with the solid solution phase changes. The resulting change in the lattice parameter is consistent with the direction in which the solid solution peaks move. The details concerning the quantification of the phases and calculation of the lattice parameters will be presented in section 4.3.6 of this chapter.

The features in the diffractograms for composition 2 and 3 will not be addressed in as much detail as composition 1 but the comparison of the XRD patterns and the tabulated summaries will be presented.

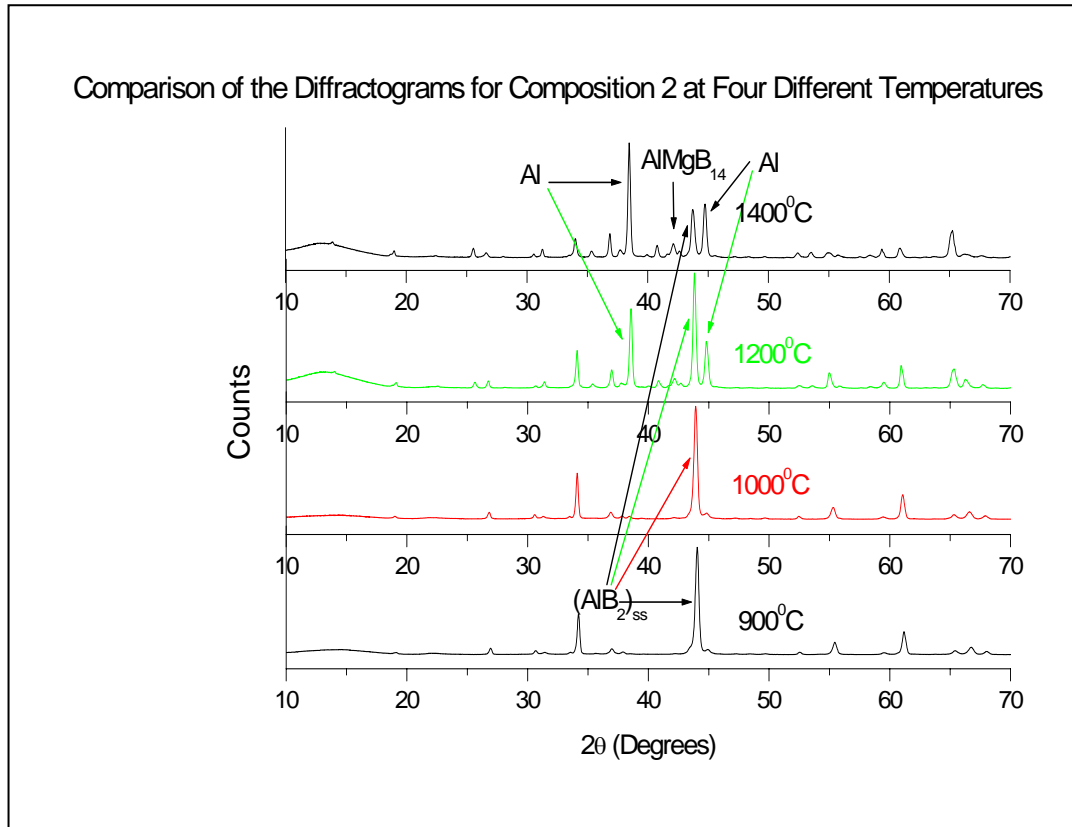


**Figure 4.3.4:** Comparison of the diffractograms for composition 2

The major peak for the solid solution phase is shifted to lower angles at higher temperatures for composition 2, as was observed for composition 1. Al and  $\text{AlMgB}_{14}$  formation occurs for temperatures above 1200°C suggesting that the solid solution boundary has not yet shifted past the composition point 2 at temperatures lower than 1200°C.

An important observation for composition 2 is that from the diffractograms the amount of Al phase present at 1200°C is less than that at 1400°C as evidenced by the ratio of the most intensive Al peak to the most intensive  $(\text{AlB}_2)_{\text{ss}}$  peak. Also the ratio of the  $(\text{AlB}_2)_{\text{ss}}$  and  $\text{AlMgB}_{14}$  major peaks decreases, suggesting that there is either less  $(\text{AlB}_2)_{\text{ss}}$  or more  $\text{AlMgB}_{14}$ . Therefore, at higher temperatures the shift in the  $2\theta$  positions of the solid solution peaks means that the solid solution is richer in Mg, see

section 4.3.6. The  $(\text{AlB}_2)_{\text{ss}}$  decomposes into Al liquid and  $\text{AlB}_{12}$  as can be seen from the binary phase diagram presented in figure 4.1.1. The XRD for composition 2 at  $1400^\circ\text{C}$  does not indicate any  $\text{AlB}_{12}$  present in the material and therefore it is possible that the presence of the liquid phase facilitates mass transport for the proposed reaction of  $\text{AlB}_{12} + 2\text{B} + \text{Mg} \rightarrow \text{AlMgB}_{14}$ . Composition 2 comprises of the phases  $(\text{AlB}_2)_{\text{ss}}$ ,  $\text{Al}_{(\text{l})}$ ,  $\text{AlMgB}_{14}$  and  $\text{MgAl}_2\text{O}_4$  at  $1400^\circ\text{C}$ .

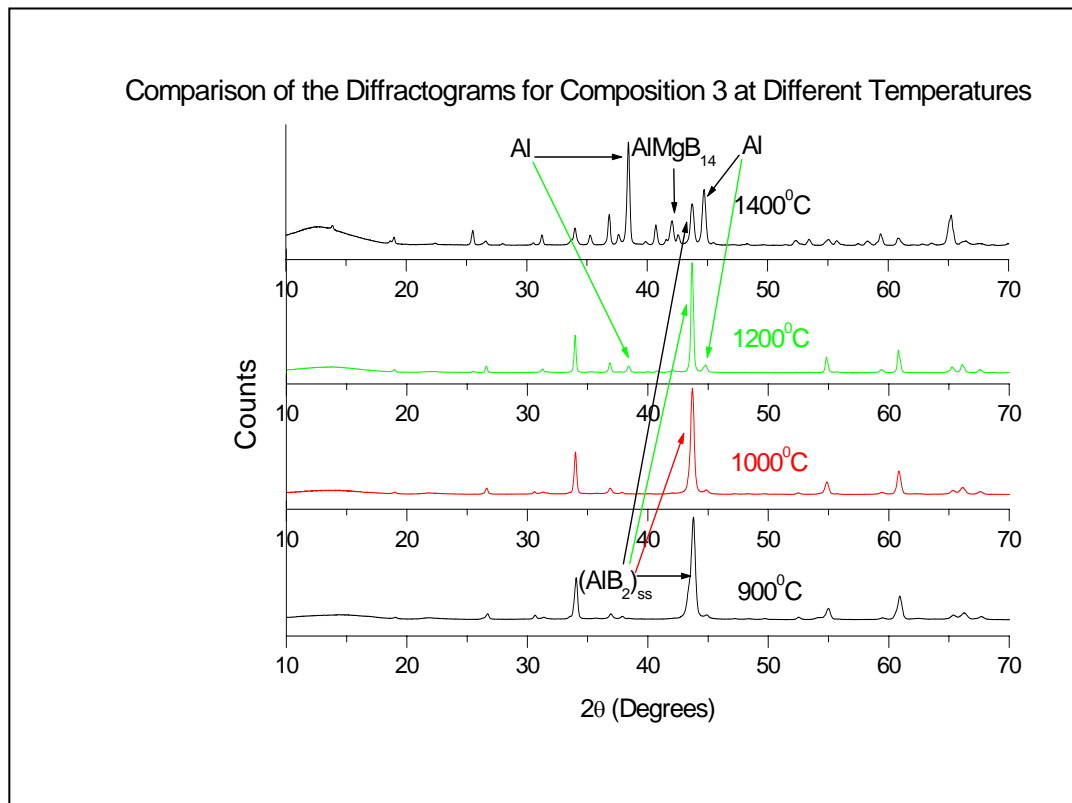


**Figure 4.3.5:** Comparison of the diffractograms for composition 3

At  $1200^\circ\text{C}$  composition 3 has a very small amount of Al. If Al and the solid solution phase are in equilibrium with each other for composition point 3 at  $1200^\circ\text{C}$  then  $\text{AlMgB}_{14}$  must be formed as well, section 4.3.6. The presence of  $\text{AlMgB}_{14}$  is not readily detected by XRD for composition 3 at  $1200^\circ\text{C}$ . This means that very little  $\text{AlMgB}_{14}$  ( $< 5 \text{ wt.}\%$ ) has formed.

A very large Al peak is visible in the diffractogram for composition 3 at  $1400^\circ\text{C}$ . Additionally, the solid solution phase,  $\text{AlMgB}_{14}$  and some spinel is also produced. As is the case for composition 1 and 2 the position of the peaks for the solid solution

phase are shifted to lower angles as the synthesis temperature of composition 3 is increased.

The ratio of the peak heights for the major Al and solid solution peaks are very similar for composition 2 and composition 3 prepared at 1400°C. The only possible explanation for this would be if the two compositions were very similar. This is not the case as is shown in table 4.3.1. Composition 3 is much richer in magnesium than composition 2. A probable explanation is that unreacted magnesium will volatilise at temperatures in excess of 1000°C, figure 4.1.2. The presence of additional magnesium in composition 3 may result in some of the unreacted Mg volatilising and thus the composition of composition 3 will become similar to composition 2. Evidence for the volatilisation of magnesium is presented below.

The volatilisation of magnesium is best understood when analysing composition 9 at the various temperatures. Composition 9, as shown in figure 4.3.1 lies on the boron rich side of the solid solution boundary. If there is no volatilisation of magnesium at temperatures above 900°C then composition 9 will always lie in a two phase region. The equilibrium for composition 9 will always be between  $\text{AlMgB}_{14}$  and the solid solution phase. Because of the position of composition 9 a tie line between  $\text{AlMgB}_{14}$  and the solid solution boundary should always give a solid solution composition rich in  $\text{MgB}_2$ , figure 4.3.6. More specifically, the composition of the solid solution will remain constant even when the solid solution boundary migrates towards  $\text{MgB}_2$ . This will be true provided that the solid solution boundary does not migrate to a point below the tie line joining  $\text{AlMgB}_{14}$  and composition point 9. This will become clear when the position of the solid solution boundary is calculated in section 4.3.6. Thus, the composition of the solid solution should remain constant for composition 9 if there is no volatilisation of magnesium.

However, if magnesium volatilises from composition 9 then this will result in the shifting of composition 9 in the general direction of composition 8, figure 4.3.1. As composition 9 is shifted in the general direction of composition 8, due to the loss of magnesium, the direction of the corresponding tie line joining  $\text{AlMgB}_{14}$  and the solid solution will change in such a way that the amount of Al in the solid solution will increase. As described in section 4.1.4 the composition of the solid solution can be

determined by the corresponding shift in the  $2\theta$  values, or d-spacings, for the solid solution phase. Table 4.3.3 tabulates the shift in the d-space for the (002) plane for the solid solution phase. Although any one of the planes could have been chosen, the (002) plane has the largest difference in d-space between  $\text{AlB}_2$  and  $\text{MgB}_2$  over the interval that the diffraction data was recorded for composition 9.

Table 4.3.2 summarises the phases that are present in composition 9 at the various temperatures.

**TABLE 4.3.2:** Summary of the major phases for composition 9

Composition		900°C	1000°C	1200°C	1400°C
9	$(\text{AlB}_2)_{\text{ss}}$ , $\text{MgAl}_2\text{O}_4$	$(\text{AlB}_2)_{\text{ss}}$ , $\text{AlMgB}_{14}$ , $\text{MgAl}_2\text{O}_4$	$\text{AlMgB}_{14}$ , $(\text{AlB}_2)_{\text{ss}}$ , $\text{MgAl}_2\text{O}_4$	$\text{AlMgB}_{14}$ , $(\text{AlB}_2)_{\text{ss}}$ , $\text{MgAl}_2\text{O}_4$	$\text{AlMgB}_{14}$ , $(\text{AlB}_2)_{\text{ss}}$ , $\text{MgAl}_2\text{O}_4$

**TABLE 4.3.3:** The shift in d-space for composition 9 at the different temperatures

Temperature (°C)	(002) plane	d-space (Å)
-	Pure $\text{MgB}_2$ : 38-1369	1.7608
900	$(\text{Al}_x\text{Mg}_{1-x})\text{B}_2$	1.7112
1000	$(\text{Al}_x\text{Mg}_{1-x})\text{B}_2$	1.7121
1200	$(\text{Al}_x\text{Mg}_{1-x})\text{B}_2$	1.6910
1400	$(\text{Al}_x\text{Mg}_{1-x})\text{B}_2$	1.6511
-	Pure $\text{AlB}_2$ : 39-1483	1.6264

The exact computation of the composition of the solid solution for composition 9 at the various temperatures was calculated, see section 4.3.7.

Table 4.3.4 summarises the phase information obtained from the qualitative XRD analysis for compositions 1-3. A summary table for the major phases present in compositions 4-6 is presented in table 4.3.5. The phases listed in table 4.3.4 and 4.3.5 are in order of decreasing amounts. The phase content is assumed from the intensity of the major peak for that particular phase.

**TABLE 4.3.4:** Summary of the major phases for compositions 1-3

Composition	900°C	1000°C	1200°C	1400°C
<b>1</b>	(AlB <sub>2</sub> ) <sub>ss</sub> , MgAl <sub>2</sub> O <sub>4</sub>	(AlB <sub>2</sub> ) <sub>ss</sub> , Al, AlMgB <sub>14</sub> , MgAl <sub>2</sub> O <sub>4</sub>	(AlB <sub>2</sub> ) <sub>ss</sub> , Al, AlMgB <sub>14</sub> , MgAl <sub>2</sub> O <sub>4</sub>	(AlB <sub>2</sub> ) <sub>ss</sub> , Al, AlMgB <sub>14</sub> , MgAl <sub>2</sub> O <sub>4</sub>
<b>2</b>	(AlB <sub>2</sub> ) <sub>ss</sub> , MgAl <sub>2</sub> O <sub>4</sub>	(AlB <sub>2</sub> ) <sub>ss</sub> , MgAl <sub>2</sub> O <sub>4</sub>	(AlB <sub>2</sub> ) <sub>ss</sub> , Al, AlMgB <sub>14</sub> , MgAl <sub>2</sub> O <sub>4</sub>	(AlB <sub>2</sub> ) <sub>ss</sub> , Al, AlMgB <sub>14</sub> , MgAl <sub>2</sub> O <sub>4</sub>
<b>3</b>	(AlB <sub>2</sub> ) <sub>ss</sub> , MgAl <sub>2</sub> O <sub>4</sub>	(AlB <sub>2</sub> ) <sub>ss</sub> , MgAl <sub>2</sub> O <sub>4</sub>	(AlB <sub>2</sub> ) <sub>ss</sub> , Al, AlMgB <sub>14</sub> , MgAl <sub>2</sub> O <sub>4</sub>	Al, (AlB <sub>2</sub> ) <sub>ss</sub> , AlMgB <sub>14</sub> , MgAl <sub>2</sub> O <sub>4</sub>

**TABLE 4.3.5:** Summary of the major phases for compositions 4-6

Composition	900°C	1000°C	1200°C	1400°C
<b>4</b>	(AlB <sub>2</sub> ) <sub>ss</sub> , Al, MgAl <sub>2</sub> O <sub>4</sub>	Al, (AlB <sub>2</sub> ) <sub>ss</sub> , AlMgB <sub>14</sub> , MgAl <sub>2</sub> O <sub>4</sub>	Al, (AlB <sub>2</sub> ) <sub>ss</sub> , AlMgB <sub>14</sub> , MgAl <sub>2</sub> O <sub>4</sub>	Al, (AlB <sub>2</sub> ) <sub>ss</sub> , AlMgB <sub>14</sub> , MgAl <sub>2</sub> O <sub>4</sub>
<b>5</b>	(AlB <sub>2</sub> ) <sub>ss</sub> , Al, MgAl <sub>2</sub> O <sub>4</sub>	(AlB <sub>2</sub> ) <sub>ss</sub> , Al, AlMgB <sub>14</sub> , MgAl <sub>2</sub> O <sub>4</sub>	Al, (AlB <sub>2</sub> ) <sub>ss</sub> , AlMgB <sub>14</sub> , MgAl <sub>2</sub> O <sub>4</sub>	Al, (AlB <sub>2</sub> ) <sub>ss</sub> , AlMgB <sub>14</sub> , MgAl <sub>2</sub> O <sub>4</sub>
<b>6</b>	(AlB <sub>2</sub> ) <sub>ss</sub> , Al, MgAl <sub>2</sub> O <sub>4</sub>	(AlB <sub>2</sub> ) <sub>ss</sub> , Al, MgAl <sub>2</sub> O <sub>4</sub>	(AlB <sub>2</sub> ) <sub>ss</sub> , Al, AlMgB <sub>14</sub> , MgAl <sub>2</sub> O <sub>4</sub>	Al, (AlB <sub>2</sub> ) <sub>ss</sub> , AlMgB <sub>14</sub> , MgAl <sub>2</sub> O <sub>4</sub>

Composition 4, 5 and 6 lie in the aluminium rich area of the ternary phase diagram. They lie adjacent to compositions 1, 2 and 3 respectively, figure 4.3.1. Compositions 4, 5 and 6 have excess aluminium and at 900°C these compositions react to form a solid solution. Therefore, the diffractograms for these three compositions indicate the solid solution phase and Al. Also at 900°C the temperature is not sufficient to allow for any volatilisation of magnesium which would result in a shift in the compositions of 4, 5 and 6.

At 1000°C the solid solution boundary moves towards higher MgB<sub>2</sub> content as discussed earlier. In composition 4 AlMgB<sub>14</sub>, Al and the solid solution are in equilibrium. The recession of the boundary results in the formation of an MgB<sub>2</sub> richer solid solution phase. At temperatures of 1200°C and 1400°C the amount of Al present is larger than the amount of solid solution which is consistent with the migration direction of the solid solution boundary. Furthermore, at temperatures in excess of 1000°C the volatilisation of magnesium becomes important as will be addressed in the discussion for the phase content in composition 5 and 6.

At 1000°C, from XRD analysis, in composition 5 AlMgB<sub>14</sub> is in equilibrium with Al and the solid solution phase. The loss of magnesium metal shifts composition 5 towards composition 4. This shifted composition point 5 is now in equilibrium with AlMgB<sub>14</sub>, Al and the solid solution at 1000°C. The solid solution phase is the phase present in the largest quantity. As the temperature is increased to 1200°C the solid solution boundary recedes further from the shifted composition 5. Together with the solid solution boundary recession at 1200°C and 1400°C and the greater volatilisation of Mg at these temperatures, the shifted composition point 5 is even further from the solid solution boundary. This results in a larger Al content at 1200°C and 1400°C.

The same explanation applies to composition 6 as was applied to composition 5. However, because of the position of composition 6 the shift in the composition point as a result of the volatilisation of magnesium pushes it to a position that is closer to the original composition point 5. Thus at 1000°C the equilibrium, for the shifted composition 6, is between Al and the solid solution phase.

At 1200°C the migration of the solid solution boundary towards MgB<sub>2</sub> and the greater amount of Mg that is volatilised results in a larger amount of Al which is seen in the diffractogram for composition 6 at 1200°C. The composition of sample 6 has shifted towards the original composition 5 and is most likely in a position, with respect to the shifted solid solution boundary, that is in equilibrium with the phases AlMgB<sub>14</sub>, Al and the solid solution phase. This accounts for the fact that less Al is present than solid solution for the shifted composition 6 at 1200°C.

At 1400°C the composition of sample 6 is further shifted due to a greater amount of volatilised magnesium. Hence, the resulting composition 6 is even further from the migrated solid solution boundary resulting in the formation of a greater amount of Al than solid solution at 1400°C.

Composition 8 lies between the solid solution and  $\text{AlMgB}_{14}$  which is in the boron rich area of the ternary phase diagram. Figure 4.3.6 indicates the diffractograms obtained for the four different temperatures.

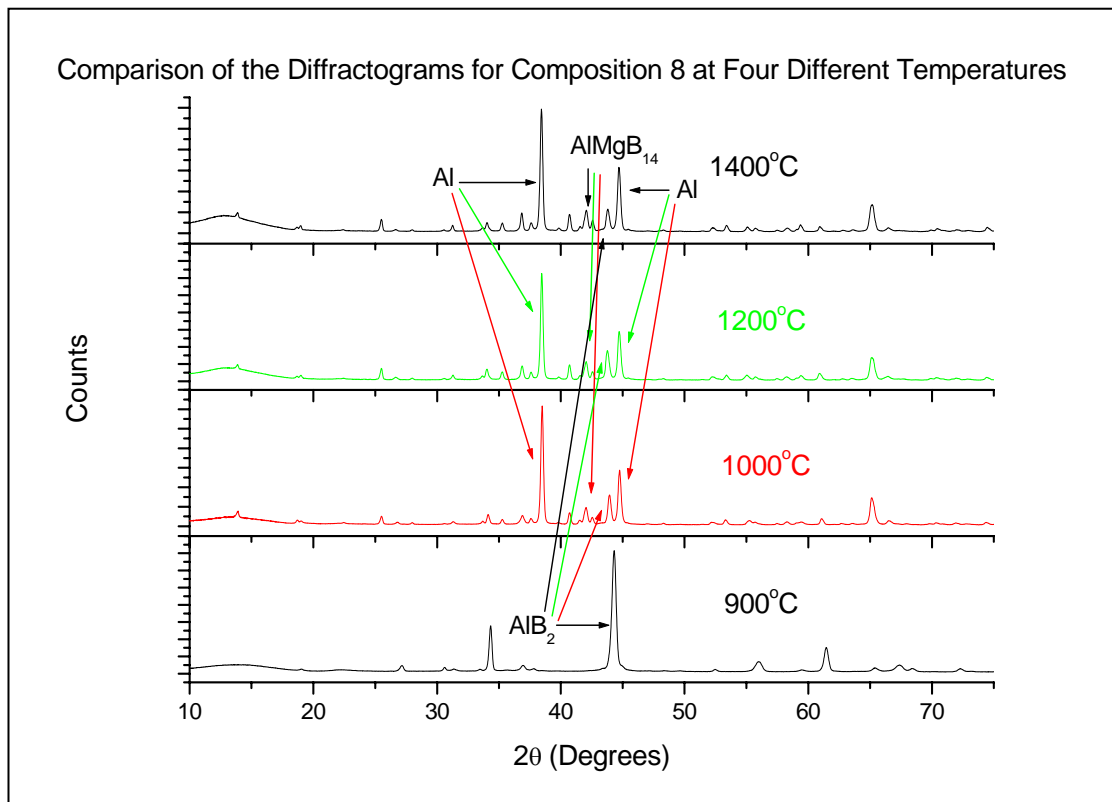


**Figure 4.3.6:** Comparison of the diffractograms for composition 8

Composition 10 corresponds to the composition  $\text{AlMgB}_{14}$ . The diffractograms of composition 10 are summarised in figure 4.3.7 and together with composition 8 the phases are tabulated in table 4.3.6.

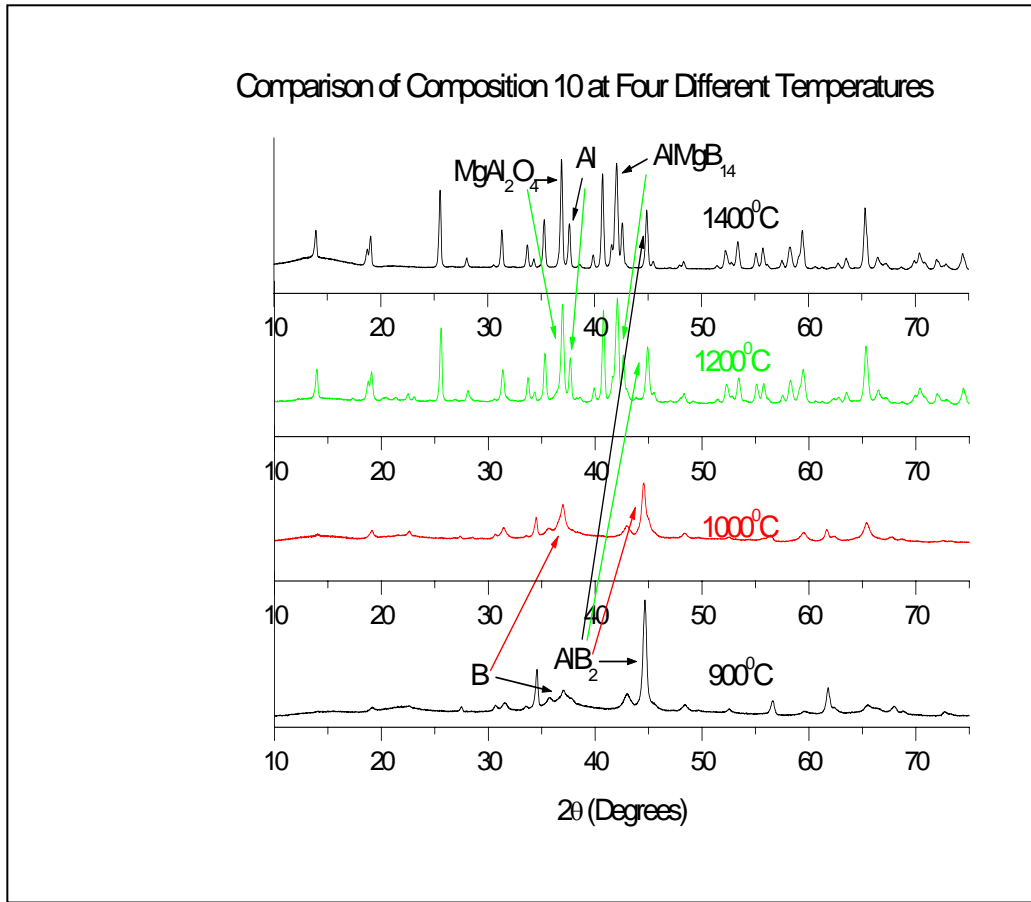


**Figure 4.3.7:** Comparison of the diffractograms for composition 10

**TABLE 4.3.6:** Summary of the major phases identified for composition 8 and 10

Temperature (°C)	Phases	
	Composition 8	Composition 10
900	(AlB <sub>2</sub> ) <sub>ss</sub> , MgAl <sub>2</sub> O <sub>4</sub>	(AlB <sub>2</sub> ) <sub>ss</sub> , B, MgAl <sub>2</sub> O <sub>4</sub>
1000	Al, (AlB <sub>2</sub> ) <sub>ss</sub> , AlMgB <sub>14</sub> , MgAl <sub>2</sub> O <sub>4</sub>	(AlB <sub>2</sub> ) <sub>ss</sub> , B, MgAl <sub>2</sub> O <sub>4</sub>
1200	Al, (AlB <sub>2</sub> ) <sub>ss</sub> , AlMgB <sub>14</sub> , MgAl <sub>2</sub> O <sub>4</sub>	AlMgB <sub>14</sub> , MgAl <sub>2</sub> O <sub>4</sub> , (AlB <sub>2</sub> ) <sub>ss</sub> , Al
1400	Al, (AlB <sub>2</sub> ) <sub>ss</sub> , AlMgB <sub>14</sub> , MgAl <sub>2</sub> O <sub>4</sub>	AlMgB <sub>14</sub> , MgAl <sub>2</sub> O <sub>4</sub> , (AlB <sub>2</sub> ) <sub>ss</sub> , Al

It is important to note that the formation of AlMgB<sub>14</sub> is predicted from the phase diagram for both compositions 8 and 10 at 900°C. The XRD data is quite clear in that no peaks are present for the AlMgB<sub>14</sub> phase for both compositions 8 and 10 at 900°C.

The  $\text{AlMgB}_{14}$  phase does appear at  $1000^{\circ}\text{C}$  for composition 8 but not for composition 10.

The explanation is that composition 8 has more aluminium than that of composition 10. This results in a larger volume of Al liquid being present in composition 8. Hence, there is better mass transport in composition 8 than in composition 10. Therefore, at  $1000^{\circ}\text{C}$  the formation of  $\text{AlMgB}_{14}$  is much more easily achieved with composition 8. The lack of formation of  $\text{AlMgB}_{14}$  at  $900^{\circ}\text{C}$  in composition 8 is due to kinetic reasons. Although the literature has reported the formation of  $\text{AlMgB}_{14}$  at  $900^{\circ}\text{C}$  for the same composition as composition 8, reaction times of 6 hours were reported. In this study a 1 hour sintering time was used. Additionally, at  $900^{\circ}\text{C}$  composition 8 readily forms a solid solution phase. This is evidenced by the lack of the Al phase at  $900^{\circ}\text{C}$ . This suggests a two step reaction. The first step involves the reaction of Al to form the solid solution  $(\text{AlB}_2)_{\text{ss}}$ .  $(\text{AlB}_2)_{\text{ss}}$  is a solid at these temperatures and thus the diffusion of aluminium and magnesium from out of the  $(\text{AlB}_2)_{\text{ss}}$  framework is restricted by kinetic reasons. Hence, the  $\text{AlMgB}_{14}$  phase is not formed after 1 hour of heating and consequently a large amount of unreacted boron is left in the mixture. The boron powder is amorphous at room temperature and semi crystalline at  $900^{\circ}\text{C}$  and is detected by the broad peaks labelled in the diffractogram for composition 10 at  $900^{\circ}\text{C}$  and  $1000^{\circ}\text{C}$ . The presence of unreacted boron in compositions similar to  $\text{AlMgB}_{14}$  have been seen under SEM and results from this sample will be presented in chapter 6.

The kinetic barrier is overcome for composition 10 at  $1200^{\circ}\text{C}$  and the appearance of crystalline  $\text{AlMgB}_{14}$  can be clearly seen in the diffractogram. This supports the above reasoning that a greater liquid phase enhances the formation of the  $\text{AlMgB}_{14}$  phase. Furthermore, as more and more  $\text{AlMgB}_{14}$  forms the amount of the solid solution phase decreases.

Further evidence supporting the migration of the solid solution boundary is obtained from the distribution of the phases at different temperatures as described for compositions 1-6, 8 and 9. Therefore the solid solution is not continuous at temperatures greater than  $1000^{\circ}\text{C}$ . Previous reports did not report the discontinuity of

the  $\text{AlB}_2$ ,  $\text{MgB}_2$  solid solution and so it is necessary to quantify the exact position of the solid solution boundary<sup>5</sup>.

### 4.3.3: The Thermodynamic Stability of the Phases

In order to assess that the phases produced by the various compositions are the equilibrium phases, some of the compositions were reheated to  $900^\circ\text{C}$  for a further 5 hours.

The compositions chosen were those richer in metal liquid phase. The additional liquid phase would enhance the mass transport during the reheating cycle and ensure that equilibrium had been achieved. Compositions 4, 5, 6 and 9 were reheated for 5 hours at  $900^\circ\text{C}$  under no load in a HIP furnace. The X-ray diffractograms are reproduced in figures 4.3.8 a, b, c, d respectively.

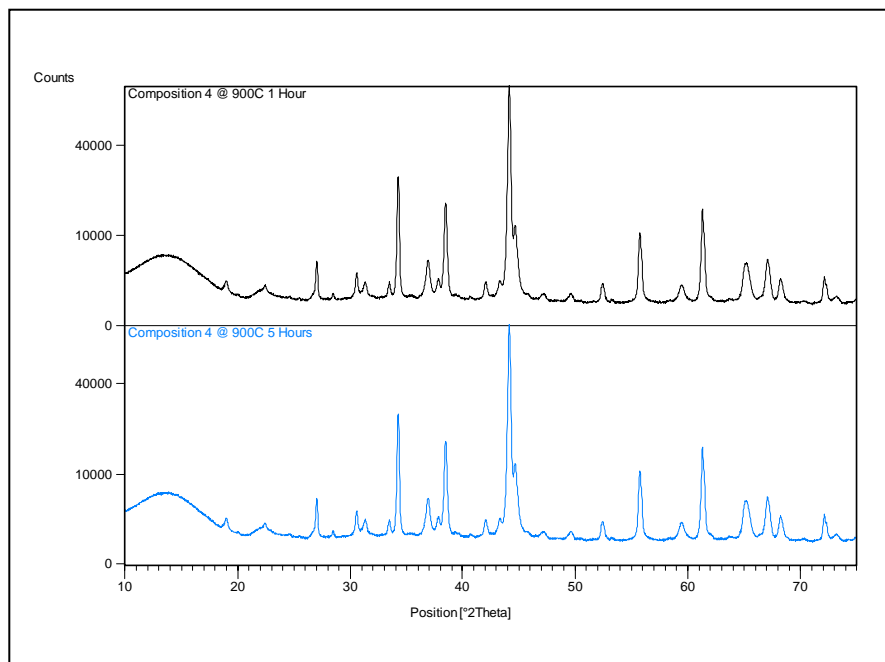


**Figure 4.3.8 a:** Composition 4 heated for 1 hour and 5 hours at  $900^\circ\text{C}$

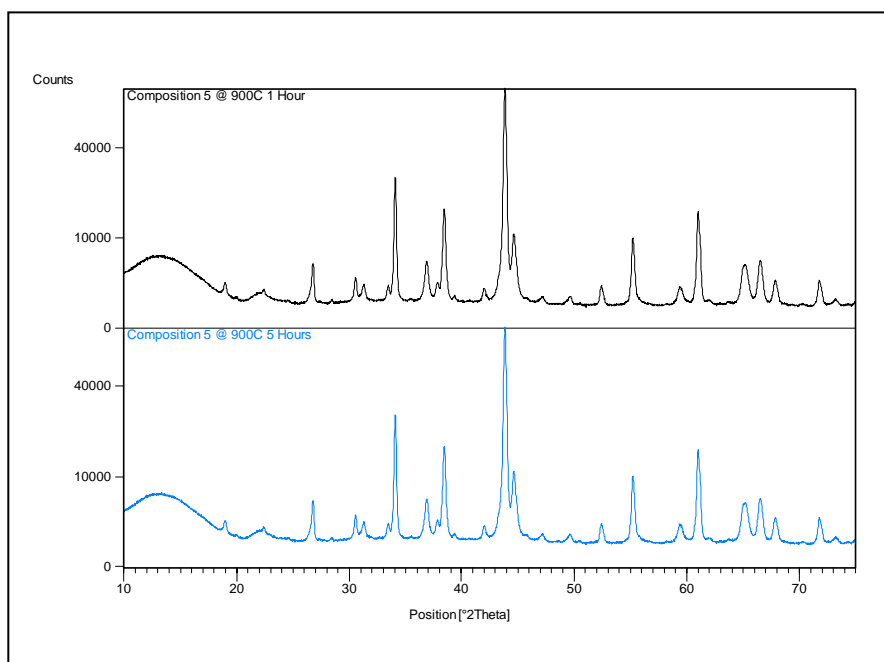


**Figure 4.3.8 b:** Composition 5 heated for 1 hour and 5 hours at 900°C

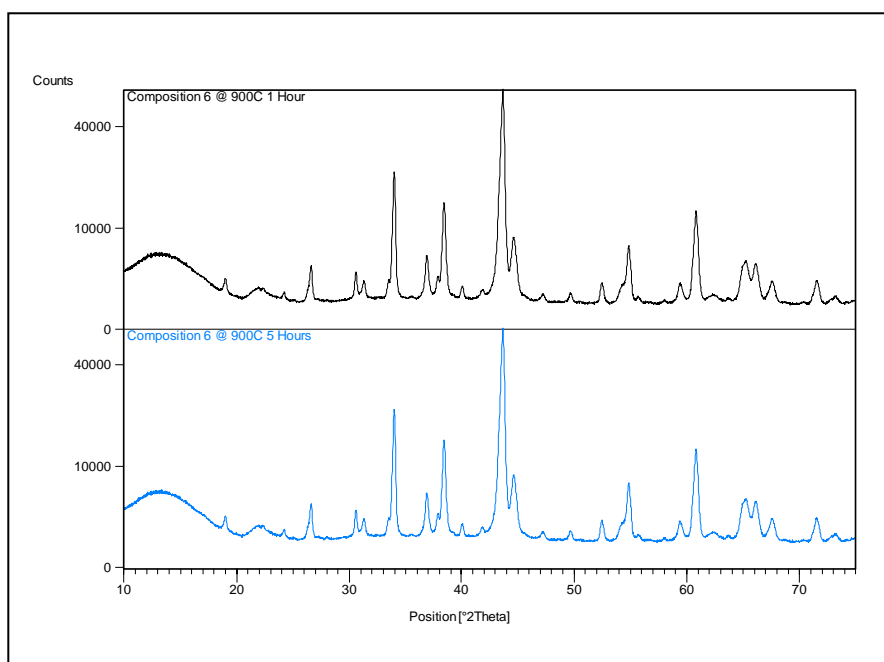


**Figure 4.3.8 c:** Composition 6 heated for 1 hour and 5 hours at 900°C

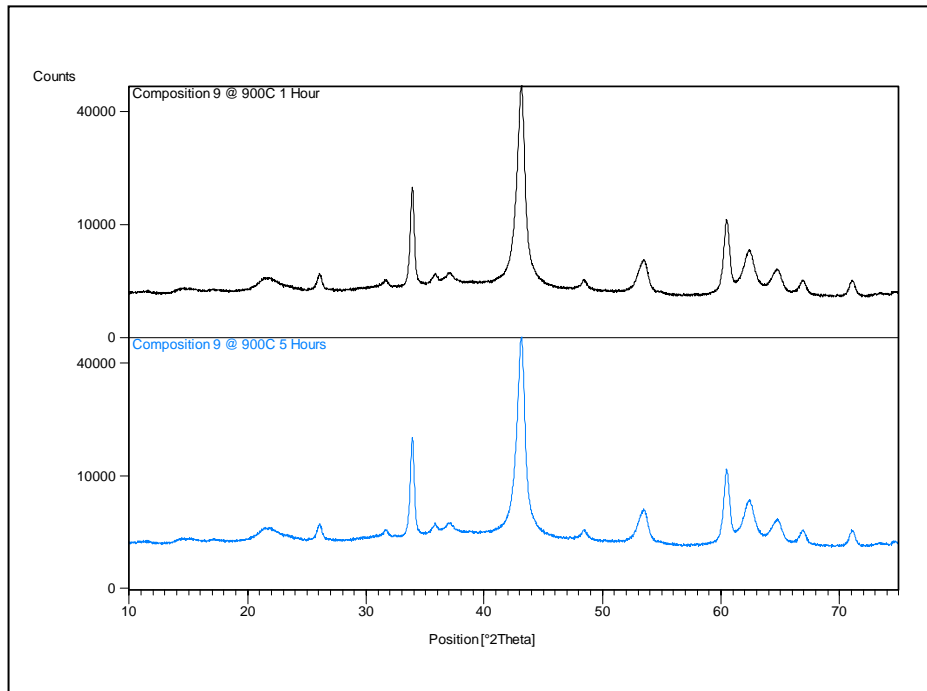


**Figure 4.3.8 d:** Composition 9 heated for 1 hour and 5 hours at 900°C

In all three compositions 4, 5 and 6 that lie on the aluminium and magnesium rich side of the solid solution boundary there is no change in the phase distribution. The appearance of no new peaks or any change in the relative intensities of the phases present for 1 hour at 5 hours means that these phases are the equilibrium phases at 900°C.

Composition 9 lies on the boron rich side of the solid solution boundary. The appearance of no new peaks in the composition at this temperature and the reproducibility of the relative intensities of the observed peaks lends further support to the fact that the phases at 900°C on both sides of the solid solution boundary retain their phases for prolonged periods of heating. However, at 900°C the formation of  $\text{AlMgB}_{14}$  from composition 9 is predicted at this temperature, figure 4.1.3. The reason for the lack of formation of larger amounts of  $\text{AlMgB}_{14}$  can only be kinetic.

Composition 8, prepared at 1200°C was reheated to 900°C for 5 hours in order to test the reversibility of the reaction,  $(\text{Al,Mg})\text{B}_2 \leftrightarrow \text{Al} + \text{AlMgB}_{14}$ . The disappearance of the major Al peak at 900°C for a sample prepared at 1200°C would be further

evidence that equilibrium had been achieved. The XRD data is presented in figure 4.3.8 e.

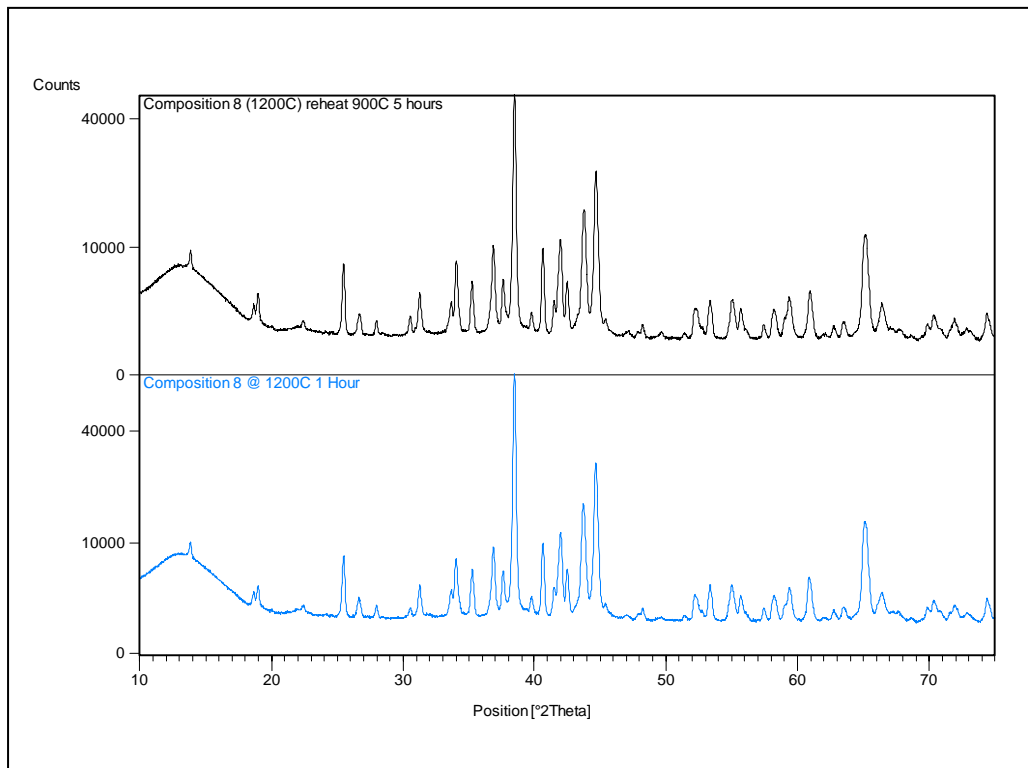


**Figure 4.3.8 e:** Composition 8 prepared at 1200°C for 1 hour and reheated for 5 hours at 900°C

The lack of the reversibility of the reaction of composition 8 prepared at 1200°C reheated to 900°C simply means that at 900°C there is insufficient time to allow for the already formed solid solution with a lower  $\text{AlB}_2$  content to reform the continuous boundary that is present at 900°C.

#### ***4.3.4: Quantifying the Phases using Rietveld Analysis***

The position of the solid solution boundary is best determined from compositions that will be in equilibrium with the phases that are in equilibrium with the solid solution boundary, i.e. Al and  $\text{AlMgB}_{14}$ . Compositions 1, 4 and 8 fulfil this criteria. This point is illustrated in figure 4.3.9. It is important to stress that figure 4.3.9 is used for illustrative purposes only.

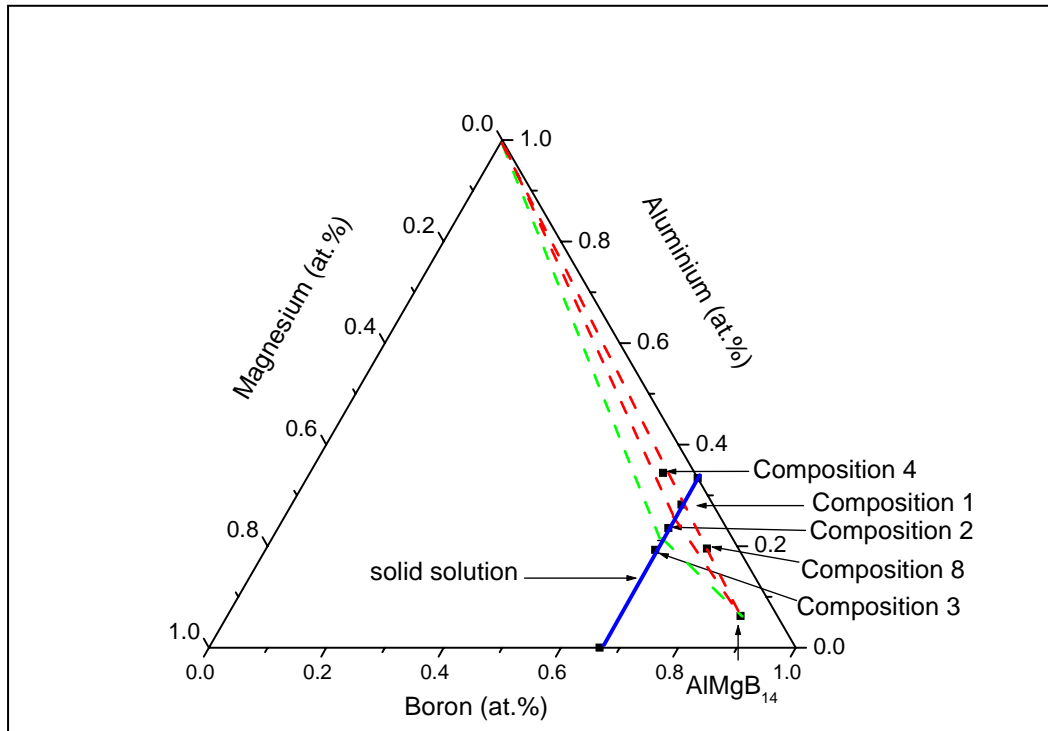


**Figure 4.3.9:** Schematic of the equilibrium phases predicted for compositions 1, 4 and 8 at the 1000°C and 1200°C temperatures

The triangle regions formed by the solid solution boundary are colour coded. The red triangle is the region formed at 1000°C and the green triangle the solid solution boundary expected at 1200°C. From the qualitative phase analysis presented in section 4.3.2 at 1000°C, Al,  $(AlB_2)_{ss}$  and  $AlMgB_{14}$  are all present for compositions 1, 4 and 8.

The Rietveld results for quantifying the phases in composition 1, 4 and 8 at 900°C and 1000°C as well as the data for composition 4 and 8 at 1200°C and 1400°C are given in Table 4.3.7. Composition 4 and 8 lie either side of the solid solution boundary.

**TABLE 4.3.7:** Rietveld analysis data for the determination of the phase content in composition 1, 4 and 8

Composition	Wt.%			
	Al	(AlB <sub>2</sub> ) <sub>ss</sub>	MgAl <sub>2</sub> O <sub>4</sub>	AlMgB <sub>14</sub>
Comp. 1 900°C	0.0	90.9 ± 2.2	6.7 ± 0.8	2,4 ± 1.0
Comp. 1 1000°C	20,5 ± 1.0	24.4 ± 1.0	7.6 ± 0.6	47.4 ± 1.6
Comp. 4 900°C	11.7 ± 0.8	79.6 ± 1.0	8.7 ± 0.6	0,0
Comp. 4 1000°C	27.7 ± 1.0	23.1 ± 1.0	8.3 ± 0.6	41.0 ± 1.6
Comp. 4 1200°C	16.5 ± 1.0	32.8 ± 1.0	10.1 ± 0.6	40.6 ± 0.5
Comp. 4 1400°C	22.5 ± 1.0	22.1 ± 1.0	9.4 ± 0.6	46.0 ± 1.9
Comp. 8 900°C	0.7 ± 0.3	92.3 ± 1.0	6.9 ± 0.6	0.0
Comp. 8 1000°C	21.4 ± 1.0	14.0 ± 0.8	8.0 ± 0.6	56.6 ± 1.5
Comp. 8 1200°C	18.3 ± 1.0	16.3 ± 0.8	8.5 ± 0.6	56.9 ± 1.5
Comp. 8 1400°C	19.5 ± 1.0	8.9 ± 0.6	7.8 ± 0.6	63.8 ± 1.5

The first information to tackle in table 4.3.7 is the amount of spinel phase that is present in each of the samples. By knowing the amount of spinel phase present in each of the compositions at the various temperatures it is possible to shift the respective composition. The reason for this shifting of the composition is that the true composition will be aluminium and magnesium deficient because of the initial assumption that the starting powders were pure. Table 4.3.8 tabulates the recalculated atomic ratios of Al, Mg and B taking into account the loss of Al and Mg due to the amount of spinel that forms at the various temperatures for compositions 1, 4 and 8.

**TABLE 4.3.8:** Atomic Percent for unshifted and spinel shifted compositions

Composition name	Unshifted Composition Atomic Percents (%)			Spinel Shifted Atomic Percents (%)			Average Spinel Shifted Atomic Percents (%)		
	Mg	Al	B	Mg	Al	B	Mg	Al	B
Comp. 1 900°C	5.39	28.19	66.47	4.73	27.28	67.99	4.69±0.06	27.22±0.09	68.09±0.15
Comp. 1 1000°C				4.65	27.16	68.20			
Comp. 4 900°C	5.38	34.43	60.19	4.47	33.38	62.15	4.44±0.08	33.34±0.09	62.22±0.18
Comp. 4 1000°C				4.52	33.44	62.04			
Comp. 4 1200°C				4.33	33.22	62.45			
Comp. 4 1400°C				4.43	33.34	62.23			
Comp. 8 900°C	5.34	19.51	75.15	4.38	18.97	76.65	4.30±0.09	18.84±0.10	76.87±0.16
Comp. 8 1000°C				4.28	18.82	76.90			
Comp. 8 1200°C				4.23	18.73	77.04			
Comp. 8 1400°C				4.29	18.84	76.87			

The effect of the shifted compositions, as a result of the loss of aluminium and magnesium due to the formation of the spinel phase, on the composition points in the Al-Mg-B ternary phase diagram is shown in figure 4.3.10. The implication for shifting the compositions is for accuracy.

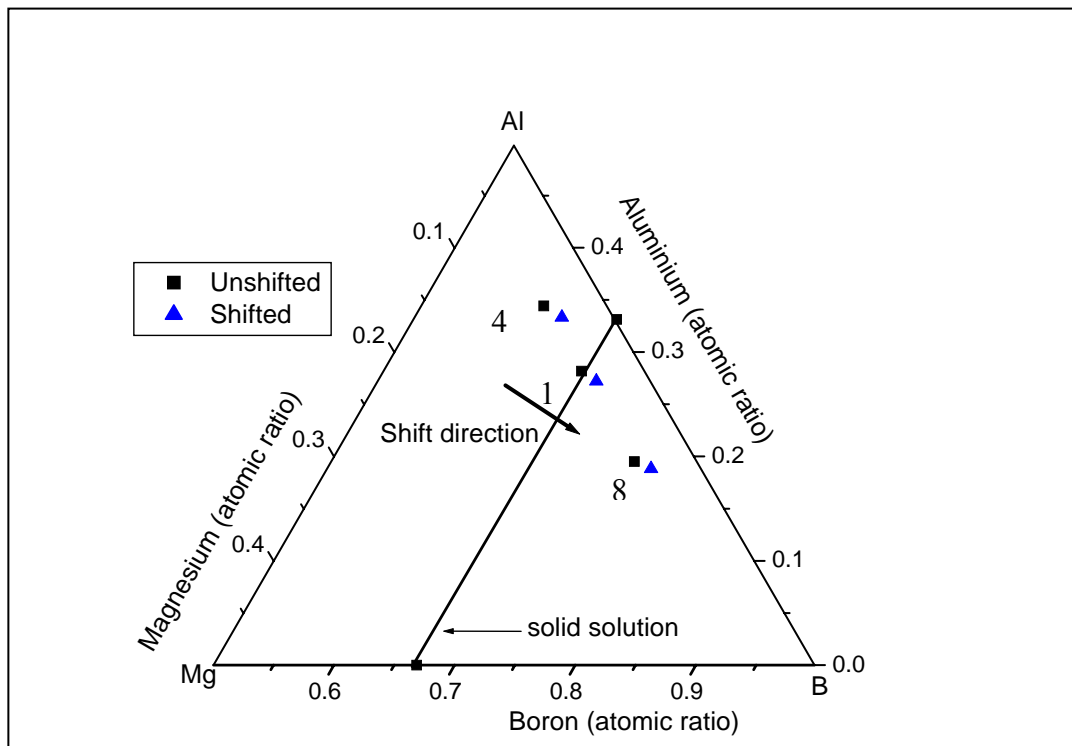


**Figure 4.3.10:** Shifted compositions 1, 4 and 8 in the ternary phase diagram

At 900°C the solid solution boundary is continuous, see figure 4.1.3. At all temperatures studied, composition 4 and 8 lie on either side of the solid solution boundary. For this reason these two compositions will be used to calculate the position of the solid solution boundary. Before calculating the position of the solid solution boundary it is important to address the issue of error bars when determining the position of the solid solution boundary.

#### **4.3.5: The Error in the 'a' and 'c' Parameter**

Vegard's law, assumes that the change in the lattice parameter is linear with respect to the amount of solute. Vegard's law is tested for composition 1, 2 and 3 at 900 and compositions 2 and 3 at 1000°C. The determined lattice parameters for the various compositions at the two different temperatures are plotted in figure 4.3.11. Tables 4.1.1 and 4.1.2 give the lattice parameters for  $\text{AlB}_2$  and  $\text{MgB}_2$  respectively.

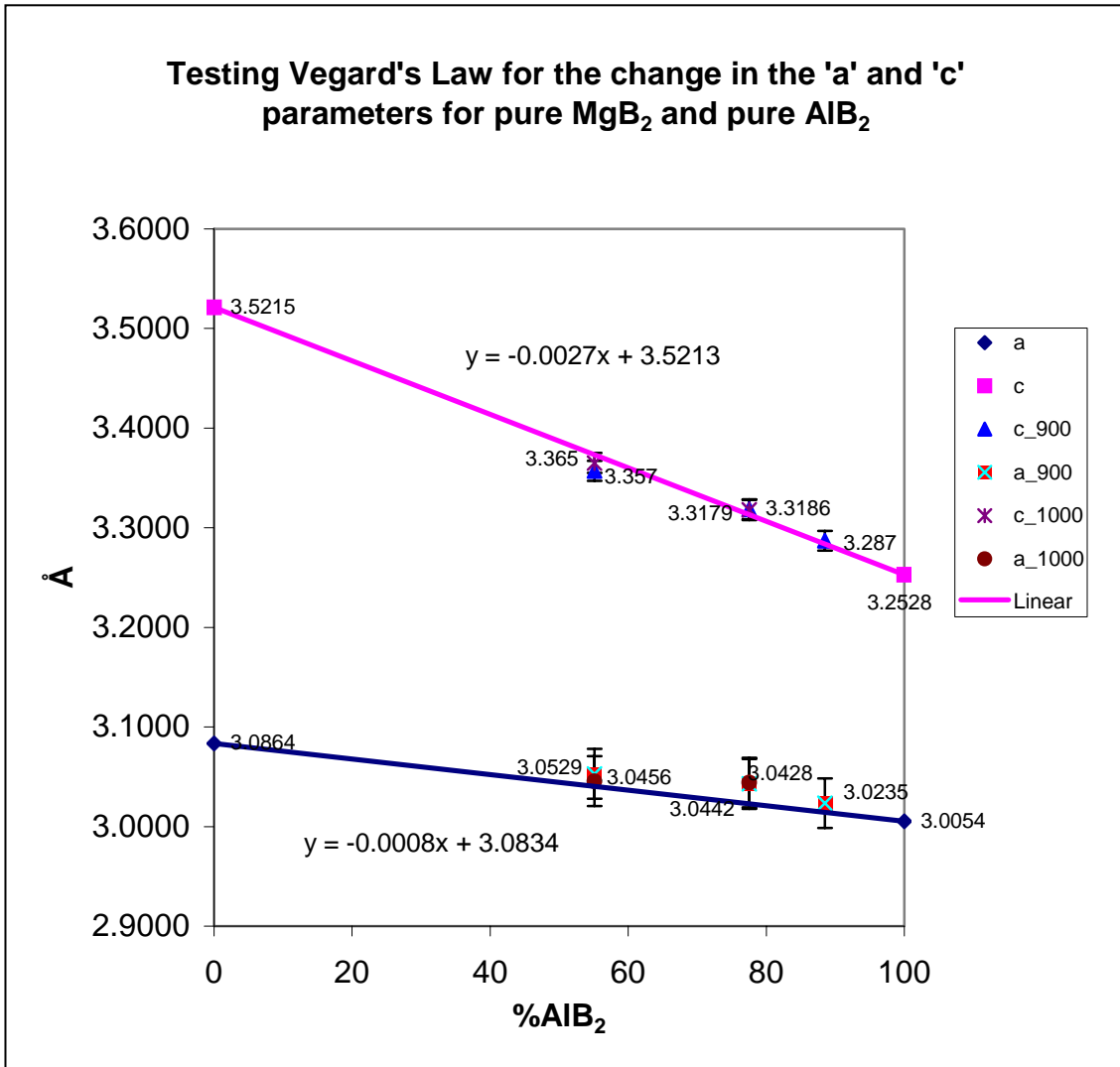


**Figure 4.3.11:** Testing Vegard's law for the change in the 'a' and 'c' parameter for pure MgB<sub>2</sub> and pure AlB<sub>2</sub>

It is clear from figure 4.3.11 that the error associated with the determination of the composition of the solid solution is more pronounced when using the 'a' parameter than when using the 'c' parameter. This is so because of the gradient associated with the line drawn in figure 4.3.11 for that parameter. The compositional error is calculated according to equation 4.3.

$$\Delta \%AlB_2 = \left(\frac{\Delta d_i}{m}\right)^2 + \left(\frac{\Delta b}{m}\right)^2 + \left(\frac{-(d_i + b)}{m} * \Delta m\right)^2 \quad 4.3$$

$d_i$  = calculated 'a' or 'c' parameter

$m$  = gradient

$b$  = intercept

By calculation  $\Delta m_{a\&c} = 2 \times 10^{-9}$ ,  $\Delta b_{a\&c} = 0.0002$ ,  $\Delta d_{i(a\&c)} = 0.0005$  (Rietveld) and  $\Delta d_{i(a\&c)} = 0.0095$  (Method 1, largest error),  $m_a = -0.0008$  and  $m_c = -0.0027$ . Hence,  $\Delta \%AlB_2 = 0.67\%$  when using the 'a' parameter and  $0.20\%$  when using the 'c' parameter. Since the gradient of the 'c' parameter is larger than the 'a' parameter the error associated with the composition of the solid solution is smaller when quantified from calculations based on the c parameter only as shown by the calculation.

#### 4.3.6: Quantifying the Solid Solution Boundary

Table 4.3.9 shows the data for the lattice parameters calculated from the Rietveld refinement.

**TABLE 4.3.9:** The calculated cell parameters from the Rietveld refinement

Sample name	(AlB <sub>2</sub> ) <sub>ss</sub>	
	a (Å)	c (Å)
Comp. 4 900°C	3.0233 ± 0.0005	3.2960 ± 0.0005
Comp. 4 1000°C	3.0357 ± 0.0005	3.3259 ± 0.0005
Comp. 4 1200°C	3.0422 ± 0.0005	3.3418 ± 0.0005
Comp. 4 1400°C	3.0409 ± 0.0005	3.3401 ± 0.0005
Comp. 8 900°C	3.0203 ± 0.0005	3.2888 ± 0.0005
Comp. 8 1000°C	3.0339 ± 0.0005	3.3232 ± 0.0005
Comp. 8 1200°C	3.0398 ± 0.0005	3.3361 ± 0.0005
Comp. 8 1400°C	3.0373 ± 0.0005	3.3327 ± 0.0005

The method of determining the solid solution boundary from the XRD data was described in the experimental section of this chapter, section 4.2.2. Table 4.3.10 are

the values of the lattice parameters calculated by using the method described in section 4.2.2. For convenience this method will be called method 1.

**TABLE 4.3.10:** Calculated lattice parameters using method 1

Sample name	$(AlB_2)_{ss}$	
	a (Å)	c (Å)
Comp. 4 900°C	3.0217 ± 0.0012	3.2937 ± 0.0030
Comp. 4 1000°C	3.0314 ± 0.0029	3.3250 ± 0.0070
Comp. 4 1200°C	3.0422 ± 0.0001	3.3454 ± 0.0020
Comp. 4 1400°C	3.0436 ± 0.0022	3.3377 ± 0.0054
Comp. 8 900°C	3.0227 ± 0.0029	3.2876 ± 0.0070
Comp. 8 1000°C	3.0326 ± 0.0028	3.3303 ± 0.0070
Comp. 8 1200°C	3.0351 ± 0.0075	3.3363 ± 0.0095
Comp. 8 1400°C	3.0400 ± 0.0014	3.3369 ± 0.0050

The lattice parameter at each temperature was converted, using Vegard's law, to %AlB<sub>2</sub> in the solid solution. Figure 4.3.12 a and b are the plotted values for the 'c' parameter for each of the compositions 4 and 8 respectively at the various temperatures. The 'c' parameter has been used for the reasons outlined in section 4.3.5. Table 4.3.11 gives the values calculated, from method 1 and the Rietveld method, for the composition of the solid solution. The different methods and the different samples give consistent results.

**TABLE 4.3.11:** Composition of the solid solution determined by Method 1 and the Rietveld method

Temperature (°C)	Composition of solid solution (%AlB <sub>2</sub> )			
	Composition 4		Composition 8	
	Method 1	Rietveld	Method 1	Rietveld
<b>900</b>	84.7	83.9	87.0	86.6
<b>1000</b>	73.1	72.8	71.1	73.8
<b>1200</b>	65.5	66.8	68.9	69.0
<b>1400</b>	68.4	67.3	68.7	70.2

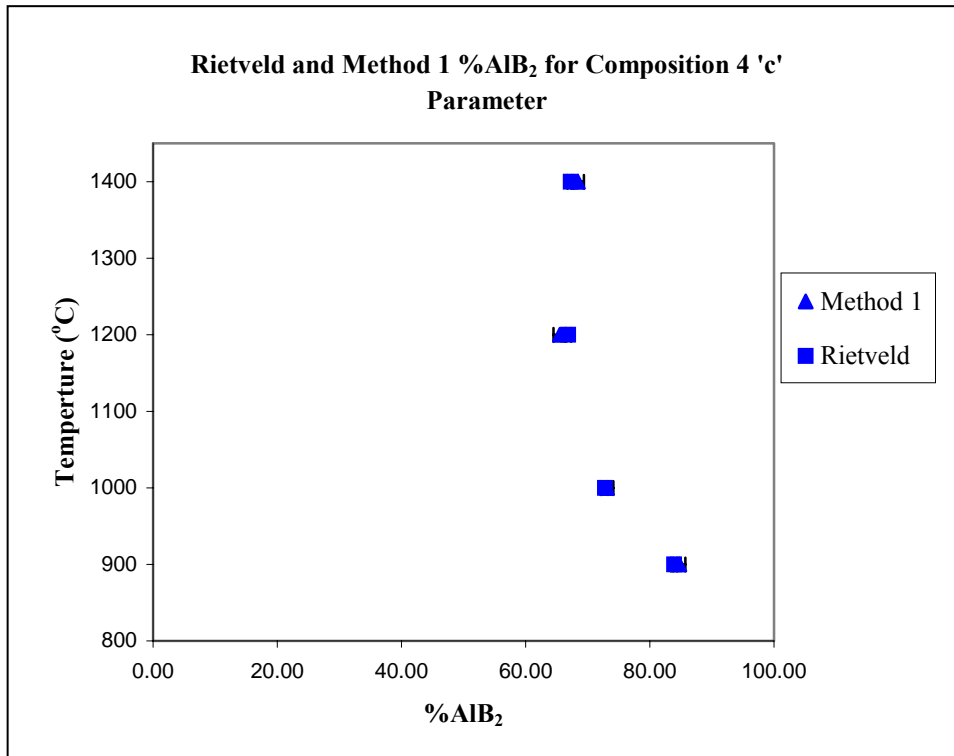


**Figure 4.3.12 a:** Rietveld and Method 1 determination of the %AlB<sub>2</sub> in the solid solution from composition 4 at 900, 1000, 1200 and 1400°C

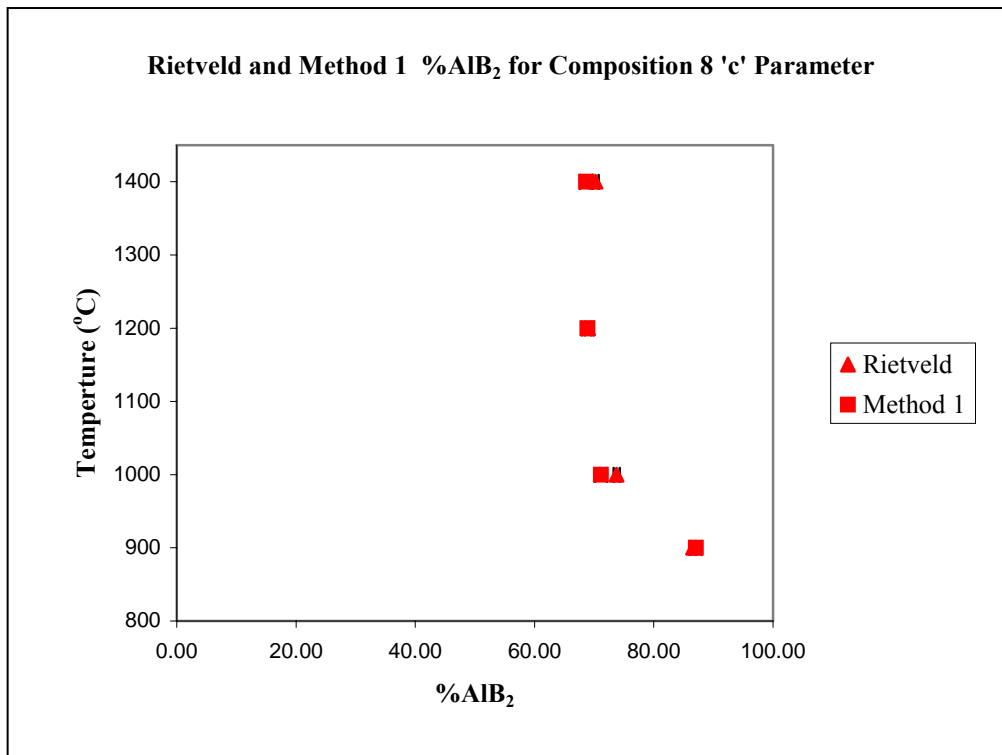


**Figure 4.3.12 a:** Rietveld and Method 1 determination of the %AlB<sub>2</sub> in the solid solution from composition 8 at 900, 1000, 1200 and 1400°C

Both method 1 and the Rietveld refinement results calculate similar amounts of  $\text{AlB}_2$  in the solid solution for compositions 4 and 8. This arises since the method used to calculate the values of the lattice parameter from the XRD data using the Rietveld method and method 1 are very similar. However, the determination of the exact peak position is much more accurately determined from the Rietveld refinement method than from method 1 due to the overlapping of peaks from different phases.

From table 4.3.7 the relative amount of solid solution present in composition 4 at the higher temperatures (1000, 1200 and 1400°C) is larger than for composition 8. Thus, the lattice parameter for the solid solution is more accurately determined from composition 4 than from composition 8. Therefore, the amount of  $\text{AlB}_2$  in the solid solution calculated from the 'c' parameter for composition 4 was used to determine the position of the solid solution boundary at 1000, 1200 and 1400°C. The composition of the solid solution at the different temperatures is shown in figure 4.3.13.

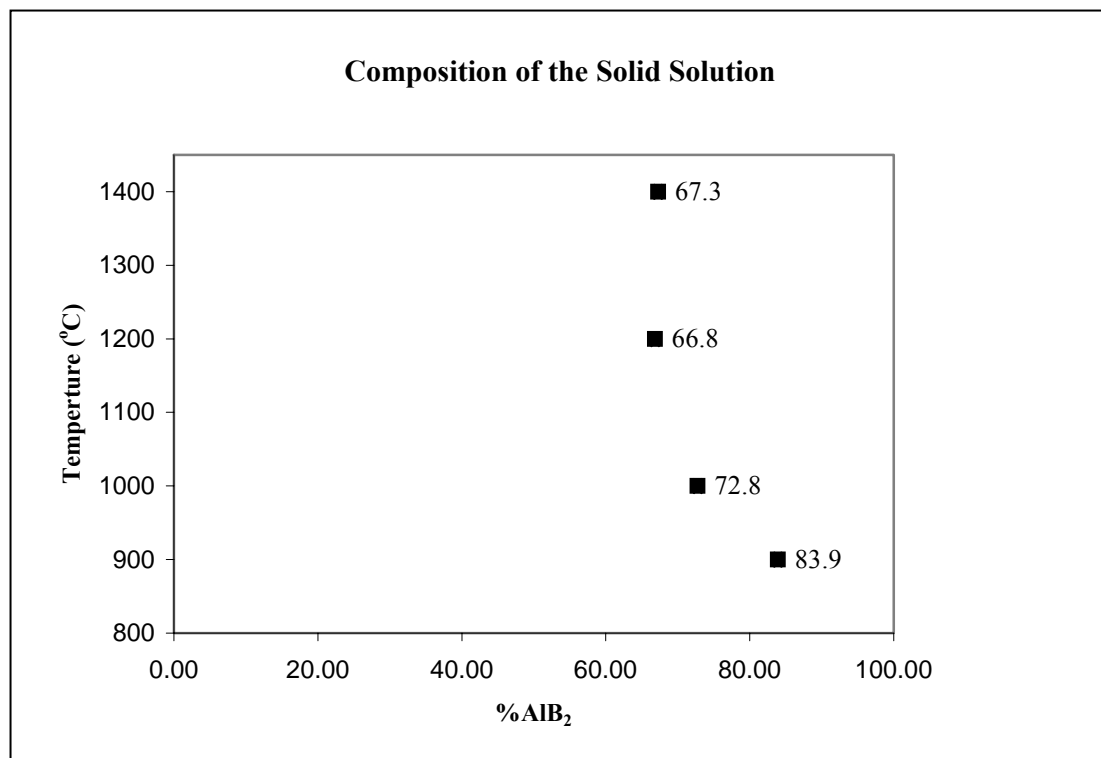


**Figure 4.3.13:** Composition of the solid solution based on the Rietveld refinement data for composition 4

### 4.3.7: Composition 9 and the Volatilisation of Magnesium

In order to explain the distribution of phases at 1200°C and 1400°C for compositions 5, 6 and 9, magnesium must volatilise at temperatures above 1000°C. By adopting the same methodology as described in section 4.2.2 the composition of the solid solution was determined for composition 9.

Table 4.3.12 tabulates the composition of the solid solution with respect to %AlB<sub>2</sub>, as calculated from the 'c' parameter, and the temperature at which such a composition exists. Figure 4.3.14 is a plot of the data presented in table 4.3.12.

**TABLE 4.3.12:** Concentration of AlB<sub>2</sub> in (AlB<sub>2</sub>)<sub>ss</sub> for composition 9 determined by method 1

Temperature (°C)	% at. AlB <sub>2</sub> ('c' parameter)	x in Al <sub>x</sub> Mg <sub>1-x</sub> B <sub>2</sub>
900	19.7	0.197
1000	33.8	0.338
1200	65.7	0.657
1400	67.9	0.679

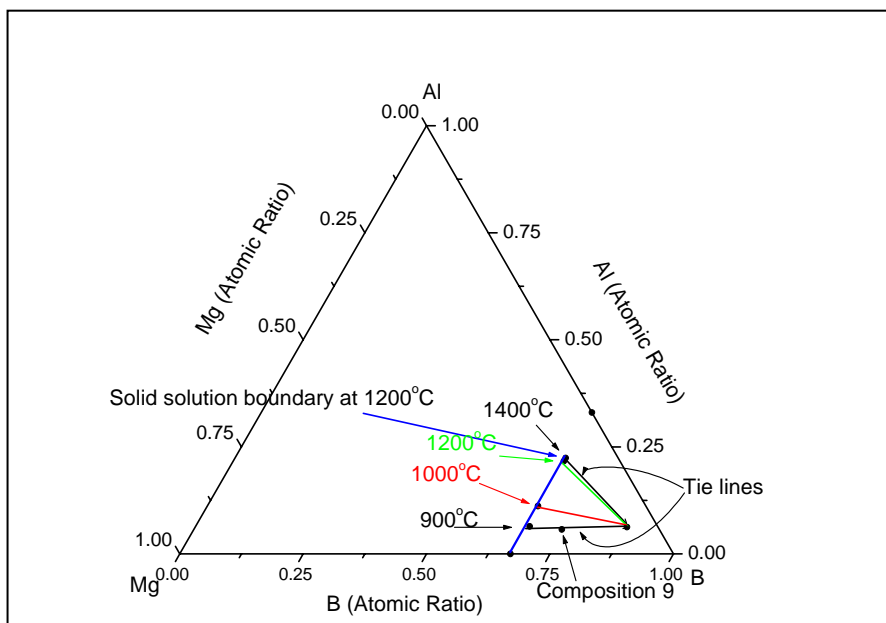


**Figure 4.3.14:** Shifted composition 9 determined from the composition of the solid solution

It is clear from figure 4.3.14 that as the temperature at which composition 9 is synthesised increases, the shift in composition 9 is towards a more magnesium deficient composition. The calculated position of the composition of the solid solution boundary from the XRD data is consistent with the shift in the solid solution composition expected from the phase analysis presented in section 4.3.2. The composition of the solid solution composition calculated at 1200°C for composition 9 is very close to the end point of the solid solution boundary as it was calculated in section 4.3.6. The fact that no Al is present in composition 9 at 1200°C and 1400°C can only mean that the composition point must lie just behind the solid solution boundary at these temperatures.

#### ***4.3.8: Verifying the Phase Content for Composition 4***

Having established the position of the solid solution boundary at temperatures of 1000, 1200 and 1400°C it is possible to check the Rietveld phase contents that were presented in table 4.3.7 for composition 4. This can be done by using tie lines in the ternary diagram for each of the phase fields formed as the solid solution boundary migrates towards MgB<sub>2</sub>.

Firstly the compositions in table 4.3.7 need to be recalculated so as to reflect the compositions assuming that the amount of spinel was zero. Table 4.3.13 reports the values of the phases formed when the amount of spinel in composition 4 is excluded.

**TABLE 4.3.13:** Composition of phases that contain all of Al, Mg and B only for composition 4 from Rietveld analysis and calculated from the starting compositions

Temperature (°C)	Al		AlB <sub>2(ss)</sub>		AlMgB <sub>14</sub>	
	Rietveld	Calc.	Rietveld	Calc.	Rietveld	Calc.
900	12.8	11.1	87.2	88.9	0.0	0.0
1000	30.2	27.8	25.2	25.0	44.6	47.2
1200	18.3	17.6	36.5	35.9	45.2	46.5
1400	24.8	22.3	24.4	28.2	50.8	49.5

The calculated values, columned under calc., presented in Table 4.3.13 have been determined from tie lines drawn in the isothermal sections for the Al-Mg-B ternary phase system. These isothermal sections are based on the position of the solid solution boundary as has been determined from composition 4 using the Rietveld method. The isothermal sections will be presented in the conclusions section of this chapter.

At 900°C composition 4 lies in a two phase region in the ternary phase diagram. A tie line drawn from Al through the spinel shifted composition 4 in table 4.3.8 yields relative amounts of 88.9% and 11.1% for  $(\text{AlB}_2)_{\text{ss}}$  and Al respectively. At 1000°C the solid solution boundary moves and the computation of the phase content for composition 4 at this temperature requires another calculation. Using the tie lines within the three phase region in which composition 4 is found at 1000°C allows for the phase content to be calculated as 47.2%, 25% and 27.8% for  $\text{AlMgB}_{14}$ ,  $\text{AlB}_2$  and Al respectively. This point is illustrated schematically in figure 4.3.15.

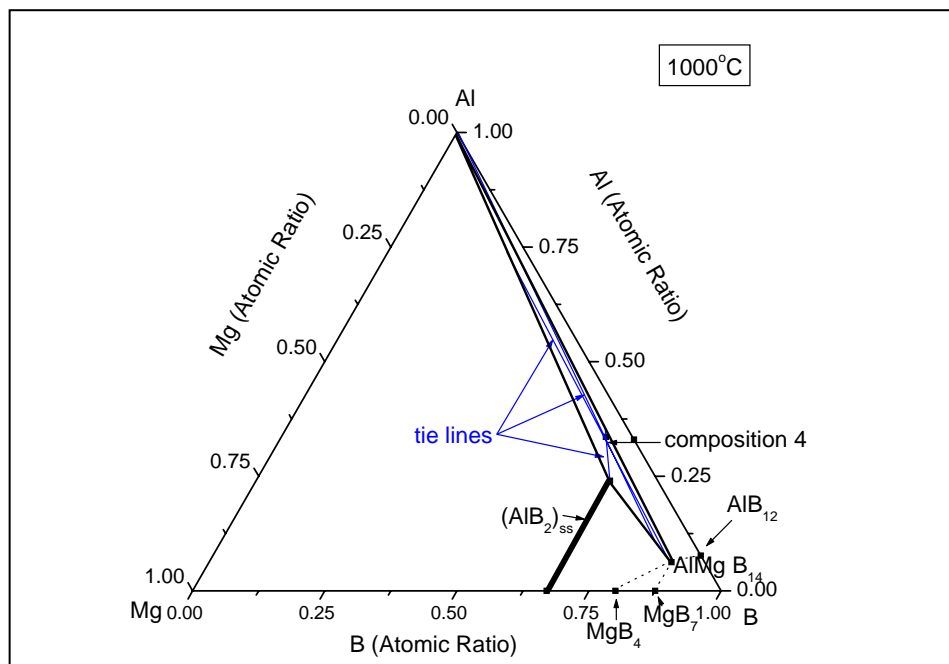


**Figure 4.3.15:** Tie lines drawn in the isothermal section of the Al-Mg-B ternary phase diagram for composition 4 at 1000°C

The agreement of the phase content from the measuring of tie lines with that computed from the Rietveld analysis is very good. This agreement confirms that at 900, 1000, 1200 and 1400°C the phases are the equilibrium phases.

#### 4.4: Summary

The phase compositions in the Al-B rich region of the Al-Mg-B ternary phase diagram were determined using qualitative and quantitative XRD analysis. Due to the oxygen content in the starting powders the determined phase diagram is a cross section through the Al-Mg-B-O quaternary phase diagram at  $3.6 \pm 0.6$  at.% O. The only stable oxide containing phase in the investigated region is  $\text{MgAl}_2\text{O}_4$ .

As a result of the volatilisation of unreacted magnesium, composition points that have excess magnesium are shifted to compositions that are richer in Al and B.

The results of the phase analysis show that at  $900^\circ\text{C}$  there exists a continuous solid solution between  $\text{AlB}_2$  and  $\text{MgB}_2$ . At temperatures of  $1000^\circ\text{C}$  and higher the solid solution is not stable in the  $\text{AlB}_2$  rich area. The boundary of the solid solution  $\text{Al}_x\text{Mg}_{1-x}\text{B}_2$  has been calculated to exist at  $x = 0.727 \pm 0.015$ ,  $0.689 \pm 0.02$  and  $0.686 \pm 0.015$  for  $1000$ ,  $1200$  and  $1400^\circ\text{C}$  respectively. The resulting isopleth through the Al-Mg-B ternary phase diagram along the 66 at.% B line is presented in figure 4.4.1.

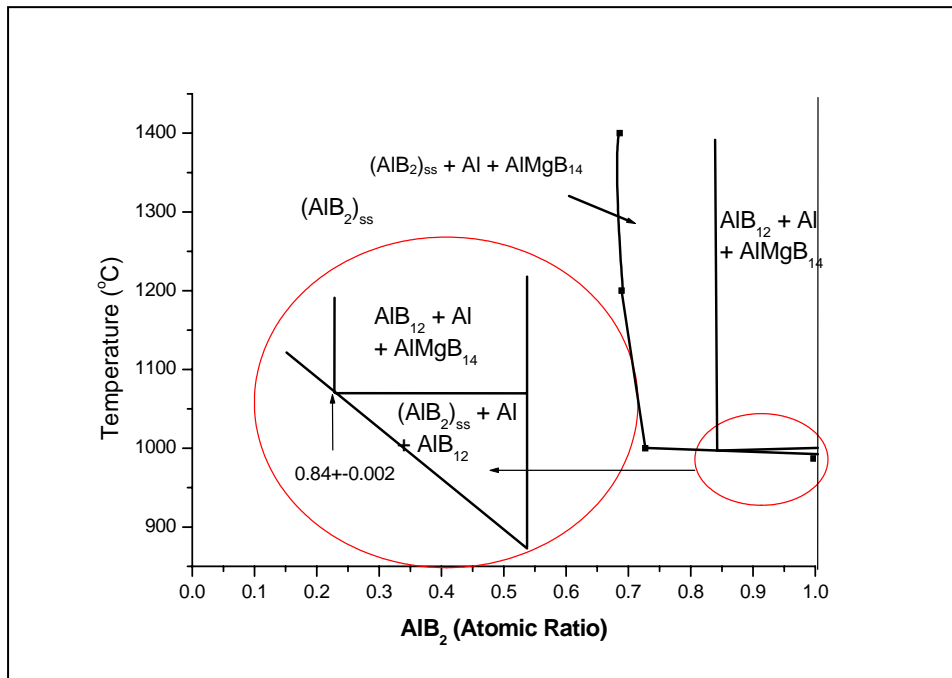


**Figure 4.4.1:** A cross section at 66 at.% B in the Al-Mg-B ternary phase diagram

Isothermal sections for the Al-Mg-B ternary diagram are given in figures 4.4.2a-c.

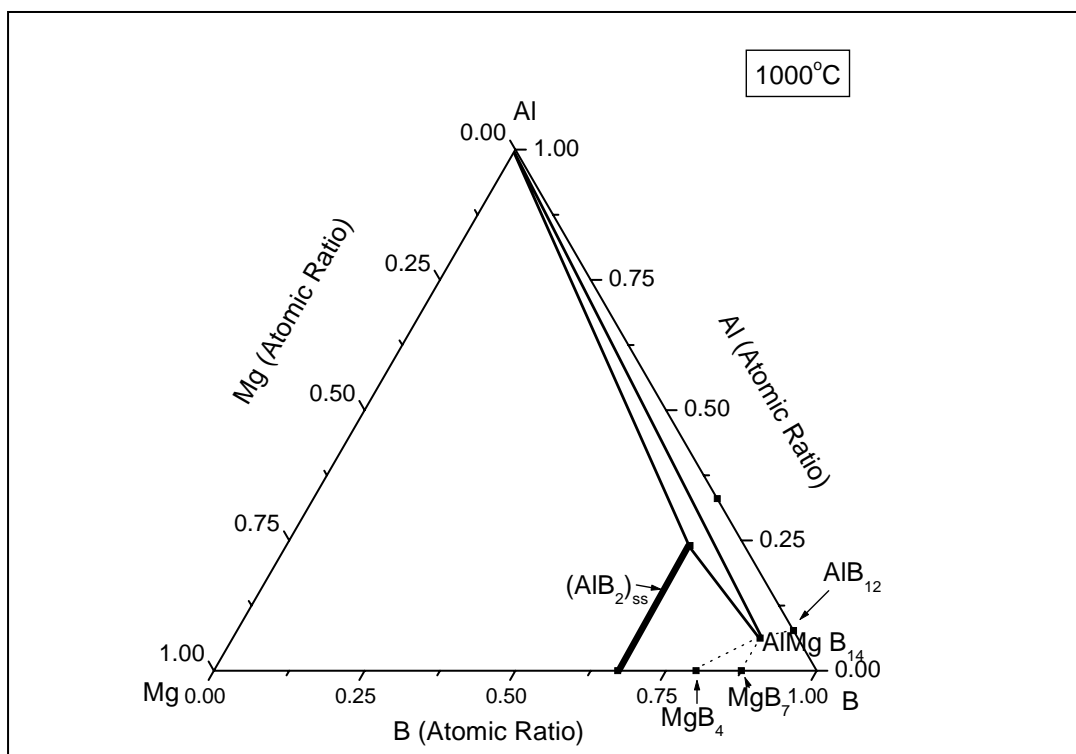


**Figure 4.4.2 a:** Isothermal section of the Al-Mg-B ternary phase diagram at 1000°C

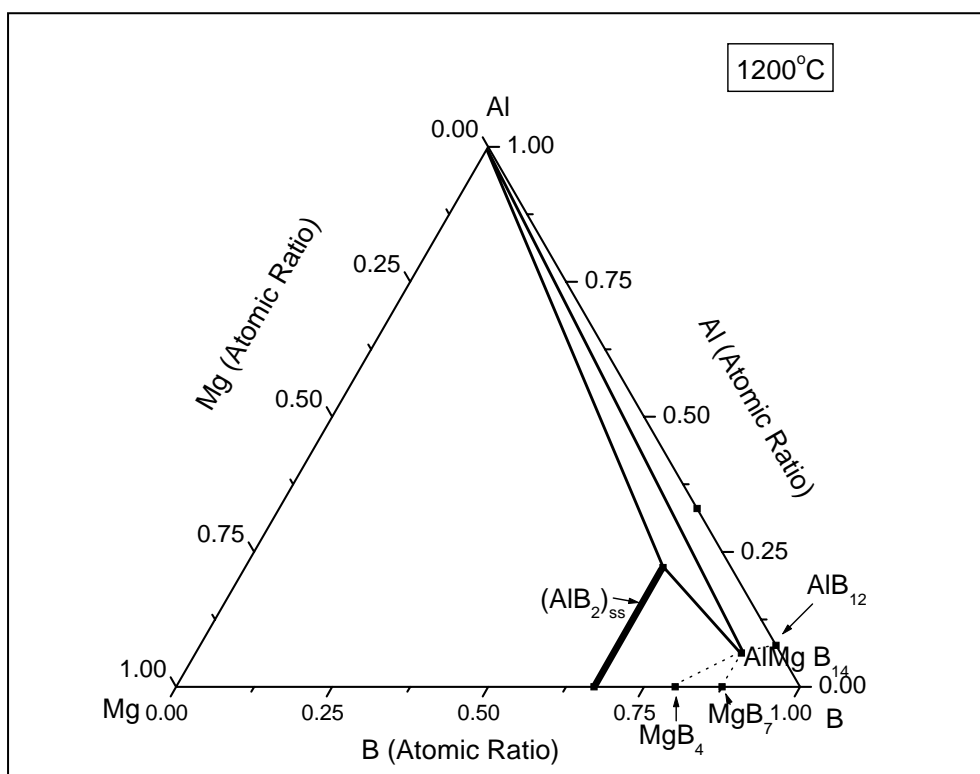


**Figure 4.4.2 b:** Isothermal section of the Al-Mg-B ternary phase diagram at 1200°C

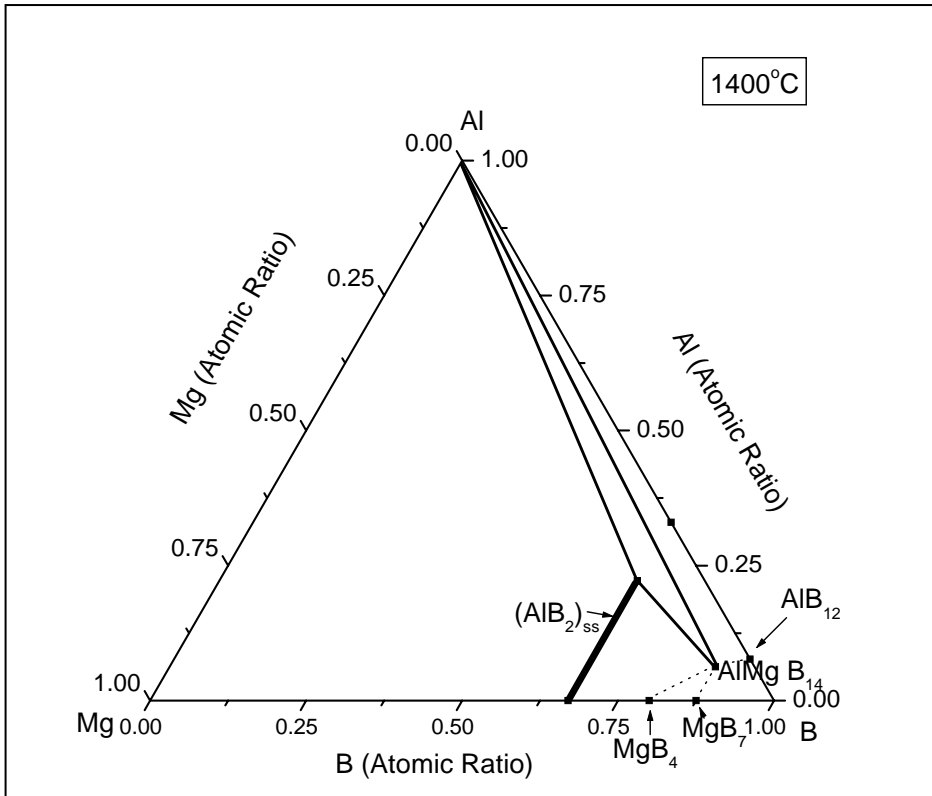


**Figure 4.4.2 c:** Isothermal section of the Al-Mg-B ternary phase diagram at 1400°C

As a result of the reduced stability of the solid solution at temperatures greater than or equal to 1000°C the phases that are in equilibrium with  $\text{AlMgB}_{14}$  changes. At temperatures below 980°C  $\text{AlMgB}_{14}$  and the solid solution are in equilibrium with each other. At temperatures  $\geq 1000^\circ\text{C}$  the solid solution decomposes and Al is formed additionally. Thus  $\text{AlMgB}_{14}$  is in equilibrium with Al and  $(\text{AlB}_2)_{\text{ss}}$ . The reaction of Al with  $\text{AlMgB}_{14}$  to form the solid solution is very slow and is not complete after 5 hours of heating at 900°C.